iScience

CellPress
OPEN ACCESS

Article

Modeling the Control of TGF-β/Smad Nuclear Accumulation by the Hippo Pathway Effectors, Taz/Yap

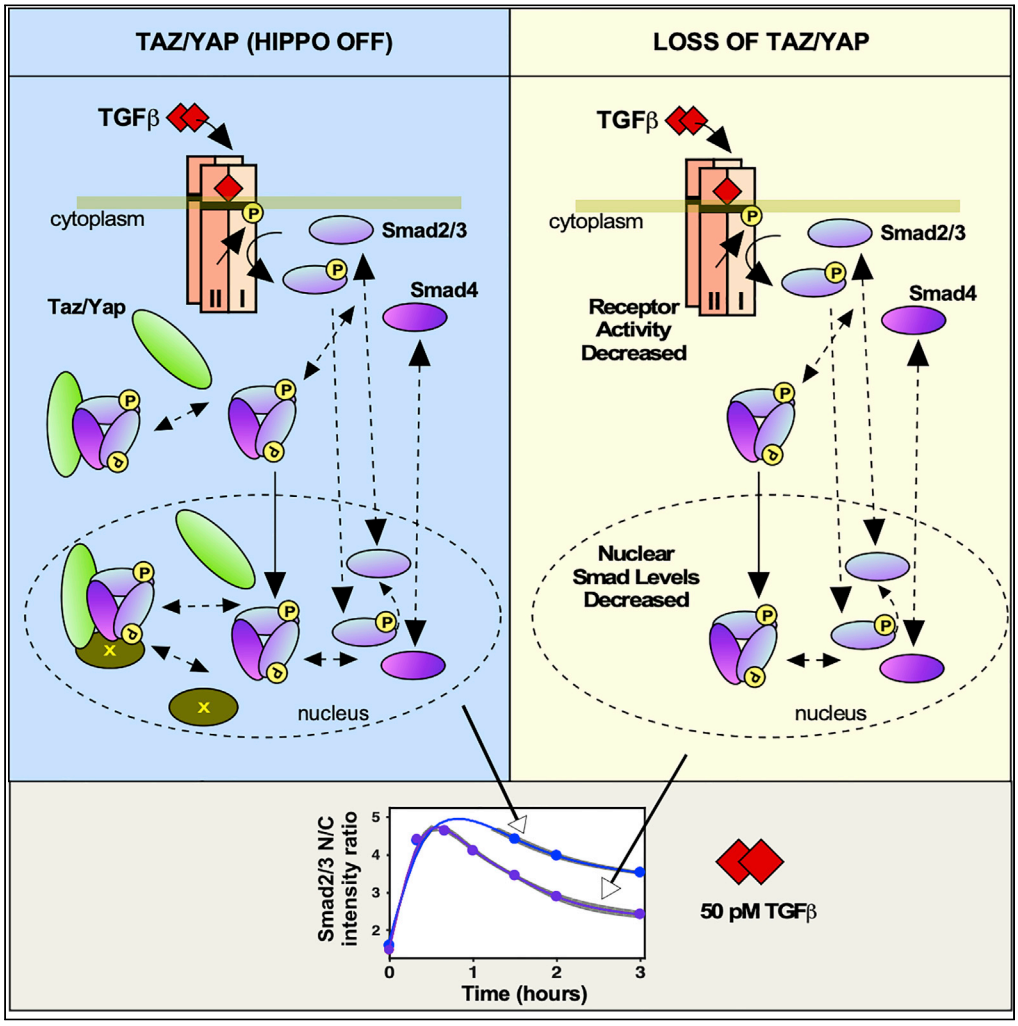

Bita Labibi, Mikhail Bashkurov, Jeffrey L. Wrana, Liliana Attisano

liliana.attisano@utoronto.ca

HIGHLIGHTS

Taz/Yap modulate TGF-β-induced nuclear accumulation of Smad2/3 and Smad4

TGF-β does not affect Taz/Yap localization when Hippo activity is constant

Taz/Yap loss may alter activity of both Receptor and Smad nuclear retention factors

The mediator complex regulates Smad nuclear accumulation

Labibi et al., iScience *23*, 101416
August 21, 2020
https://doi.org/10.1016/j.isci.2020.101416

iScience

CellPress
OPEN ACCESS

Article

Modeling the Control of TGF-β/Smad Nuclear Accumulation by the Hippo Pathway Effectors, Taz/Yap

Bita Labibi,[1,2] Mikhail Bashkurov,[3] Jeffrey L. Wrana,[3,4] and Liliana Attisano[1,2,5,*]

SUMMARY

Integration of transforming growth factor β (TGF-β) signals with those of other pathways allows for precise temporal and spatial control of gene expression patterns that drive development and homeostasis. The Hippo pathway nuclear effectors, Taz/Yap, interact with the TGF-β transcriptional mediators, Smads, to control Smad activity. Key to TGF-β signaling is the nuclear localization of Smads. Thus, to investigate the role of Taz/Yap in Smad nuclear accumulation, we developed mathematical models of Hippo and TGF-β cross talk. The models were based on experimental measurements of TGF-β-induced changes in Taz/Yap and Smad subcellular localization obtained using high-throughput immunofluorescence (IF) imaging in the mouse mammary epithelial cell line, EpH4. Bayesian MCMC DREAM parameter estimation was used to quantify the uncertainty in estimates of the kinetic parameters. Variation of the model parameters and statistical analysis show that our modeling predicts that Taz/Yap can alter TGF-β receptor activity and directly or indirectly act as nuclear retention factors.

INTRODUCTION

Signal transduction pathways translate extracellular information to define cell outcomes. Signaling cross talk allows for plasticity and versatility in cellular responses and is essential for coordinating complex biological processes such as tissue patterning (McNeill and Woodgett, 2010; Attisano and Wrana, 2013; Beyer et al., 2013). Transforming growth factor β (TGF-β) superfamily members control a myriad of cellular activities including cell growth, cell differentiation, apoptosis, cellular homeostasis, and other cellular functions (Attisano and Wrana, 2002; Shi and Massague, 2003; Hata and Chen, 2016; Hill, 2016; Budi et al., 2017). TGF-β superfamily members are noted for their function as morphogens, in which gradients of ligand control the magnitude and timing of target gene activation that ultimately establishes cell fate. TGF-β ligand initiates canonical TGF-β signaling, which results in receptor activation. Smad2/3 interact with and are phosphorylated by receptor type I and then form a complex with Smad4, the pSmad2/3-Smad4 complex. The pSmad2/3-Smad4 complex translocates into the nucleus, binds to various proteins and DNA to regulate transcription (Attisano and Wrana, 2002; Shi and Massague, 2003; Feng and Derynck, 2005; Hata and Chen, 2016; Hill, 2016; Budi et al., 2017).

Proper development requires that cells also integrate signals from other pathways, such Hippo, a major regulator of tissue growth and organ size (Genevet and Tapon, 2011; Halder and Johnson, 2011; Barry and Camargo, 2013; Park and Guan, 2013; Yu et al., 2015; Misra and Irvine, 2018; Ma et al., 2019). Cues such as high cell density activate the Hippo pathway in which a core kinase cassette phosphorylates the transcriptional regulators, Taz/Yap, driving their cytoplasmic retention and inhibiting their transcriptional activities. Hippo and TGF-β pathways are intimately interconnected (Mauviel et al., 2012; Attisano and Wrana, 2013; Beyer et al., 2013). Taz/Yap interact with activated Smads, and when Hippo is active, cytoplasmically localized Taz/Yap binds and inhibits Smad nuclear accumulation and dampens TGF-β-induced transcription (Varelas et al., 2008; Varelas et al., 2010; Beyer et al., 2013; Narimatsu et al., 2015; Maiwald et al., 2016; Narimatsu et al., 2016). The key factor in TGF-β Smad signaling pathway is Smad nuclear accumulation. Indeed, precise nuclear concentration of Smads determines which genes are turned on and thus results in the specification of diverse cell fates (Gurdon and Bourillot, 2001; Schmierer and Hill, 2007; Strasen et al., 2018). However, the regulation of Smad nuclear accumulation is still poorly understood (Clarke et al., 2006; Clarke and Liu, 2008). Two hypotheses have been put forth to explain nuclear accumulation of

[1]Department of Biochemistry, University of Toronto, Toronto, ON M5S 1A8, Canada

[2]Donnelly Centre, University of Toronto, Toronto, ON M5S 3E1, Canada

[3]Lunenfeld-Tanenbaum Research Institute, Mount Sinai Hospital, Toronto, ON M5G 1X5, Canada

[4]Department of Molecular Genetics, University of Toronto, Toronto, ON M5S 1A8, Canada

[5]Lead Contact

*Correspondence: liliana.attisano@utoronto.ca

https://doi.org/10.1016/j.isci.2020.101416

Smads. In one, it is postulated that the different forms of Smads have different kinetics of nuclear import and export, such that the phosphorylated Smads accumulate in the nucleus (Schmierer and Hill, 2005; Hill, 2009). The second proposes that there are retention factors in the nucleus that have a higher affinity for phosphorylated Smads (Hoodless et al., 1999; Xu et al., 2002; Kang et al., 2003; Nicolás et al., 2004; ten Dijke and Hill, 2004; Xu, 2006; Hill, 2009). Thus, to understand signaling cross talk between Taz/Yap-mediated Hippo and TGF-β Smad signaling pathways, it is first necessary to investigate the role of Taz/Yap in Smad nuclear accumulation. However, given the many variables, gaining a broad understanding of how TGF-β/Hippo cross talk alters Smad nuclear accumulation is extremely challenging using only biological approaches.

The interplay of mathematical modeling with experiments is one of the central elements in systems biology, an approach that has been applied to the study of TGF-β/Smad signaling (Clarke et al., 2006; Zi and Klipp, 2007; Clarke and Liu, 2008; Schmierer et al., 2008; Zi et al., 2011; Strasen et al., 2018). Indeed, computational modeling of signaling cross talk can provide insights into the complex process and accept or reject proposed scenarios. A core part of mathematical modeling is estimating unknown parameters. The main problems for modeling of biological systems are uncertain parameters and noisy measurements, and so nonlinear optimization methods may not perform well to overcome the issues of trapping in local minima and convergence of the parameter estimation algorithm (Villaverde and Banga, 2014; Vrugt, 2016). Another option is Bayesian inference, which is based on the application of Bayes' theorem, which states that the posterior distribution of a parameter is proportional to the parameter's prior distribution multiplied by a likelihood function. Bayesian methods, and particularly Markov Chain Monte Carlo (MCMC) techniques, are extremely useful in uncertainty assessment and parameter estimation of biological models (Stuart, 2010; Kirk et al., 2016). Many MCMC approaches have been implemented to solve Bayesian inference problems (Craiu and Rosenthal, 2014). Among them, the scheme entitled Differential Evolution Adaptive Metropolis or DREAM has shown to be generally superior to other MCMC sampling approaches in various cases involving nonlinearity, high-dimensionality, and multimodality (Vrugt et al., 2008a; Vrugt et al., 2009). The DREAM strategy runs multiple different Markov chains simultaneously for global exploration and automatically tunes the scale and orientation of the proposal distribution in randomized subspaces during the search (Vrugt, 2016). This strategy deals very well with uncertainty and, if designed appropriately, avoids sensitivity to initial values and resolves convergence problem. In addition, it gives probability distributions instead of single values for unknown parameters, which makes comparing the parameters more meaningful (Vrugt et al., 2008a; Vrugt et al., 2009).

As experimental data are not perfect and models contain many unknown parameters, the structural identifiability of models must be investigated (Raue et al., 2009). To infer how well model parameters are estimated by the experimental data, here, we used the profile likelihood, a data-based method to detect structural and practical non-identifiability for reducing nonlinear models and designating likely candidates for reduction (Maiwald et al., 2016). By this approach, confidence intervals, which contain the true value of the parameter with a desired probability, and as a result appropriate prior distributions for unknown parameters in the MCMC algorithm can be derived. Experimental data and statistical analysis revealed that the level of Taz/Yap in the cytoplasm or nucleus is constant regardless of dose or time of TGF-β treatment, as long as Hippo pathway activity does not change. Mathematical modeling first showed that Taz/Yap is not involved in nuclear import of the phosphorylated Smad2/3 (pSmad2/3)-Smad4 complex. Next, we developed five mathematical models of Hippo and TGF-β cross talk to test diverse hypotheses including receptor activity alterations and/or the existence of nuclear retention factors to protect the Smad complex against nuclear phosphatases. Using the Bayesian model averaging (BMA) strategy (Vrugt et al., 2008b) to discriminate the five models, the best model was selected. This work showed that Taz/Yap was not involved in changing the rate of Smad import or export or in the molecular mechanism whereby Smad is phosphorylated. Rather, the modeling predicts that Taz/Yap alter Smad nuclear accumulation by acting either directly or indirectly as a retention factor and by altering TGF-β receptor activity through a post-translational mechanism.

RESULTS

Taz/Yap Modulate the Nuclear Accumulation of Smad2/3 and Smad4

The precise nuclear concentration of Smads determines which genes are transcriptionally activated (Shi and Massague, 2003; Clarke et al., 2006; Zi et al., 2011; Hata and Chen, 2016). Two mechanisms have been proposed to explain nuclear Smad accumulation, namely, different nucleocytoplasmic shuttling

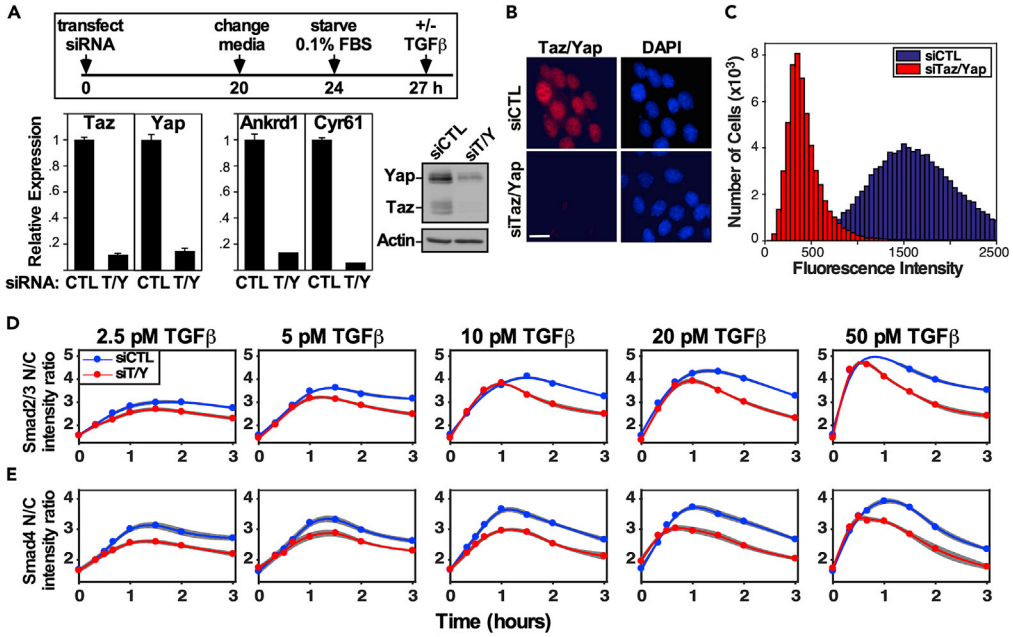

Figure 1. Analysis of the Nuclear Accumulation of Smad2/3 and Smad4 upon Loss of Taz/Yap Expression

(A) A schematic of the optimized protocol for knocking down Taz and Yap using siRNAs in EpH4 cells is shown (top). The efficiency of knocking down Taz/Yap and the reduction in expression level of the Taz/Yap target genes, Ankrd1 and Cyr61, was determined by qPCR with data plotted as the mean ± standard deviation of three independent experiments (left). Taz/Yap knockdown was confirmed by immunoblotting (right).

(B) Taz/Yap knockdown was verified by immunofluorescence microscopy.

(C) EpH4 cells were transfected with siCTL or siTaz/Yap and seeded in a 96-well plate. The localization of Taz/Yap in cells co-stained with DAPI was determined by immunofluorescence microscopy. The histogram from a representative experiment shows the intensity of Taz/Yap in transfected cells. Note that background intensity in the absence of cells is approximately 200–300 units, indicating a potent knockdown was achieved in the majority of cells.

(D and E) EpH4 cells transfected with siCTL or siTaz/Yap in 96-well plates were treated with different doses of TGF-β for varying times. Cells were fixed, nuclei visualized with DAPI, and Smad proteins stained with antibodies against Smad2/3 (D) or Smad4 (E) and visualized by immunofluorescence microscopy. Images were taken by confocal microscopy using In Cell Analyzer 6000. Smad protein localization of ~1,000 cells/well was quantified by automated image analysis. The mean (full circles) ± standard error of the mean (SEM, gray area) from at least nine independent biological experiments is shown.

kinetics for activated and inactive Smads (Schmierer and Hill, 2005; Hill, 2009) or the presence of nuclear retention factors (ten Dijke and Hill, 2004; Xu, 2006). Neither mechanism alone can completely account for existing data; thus, how Smad nuclear accumulation is regulated remains unclear. Hippo pathway activity impacts Smad activity; thus, to investigate the contribution of the Hippo pathway mediators, Taz/Yap to Smad function, we used EpH4, a TGF-β-responsive, normal mouse mammary epithelial cell line that has retained an intact Hippo pathway (Narimatsu et al., 2016) as a system to study TGF-β and Hippo cross talk. We first established experimental conditions to perturb the process in these cells by removing Taz/Yap from the nucleus by abrogating expression of both Taz and Yap using small interfering RNAs (siRNAs) (Figure 1A). The efficiency of knocking down Taz/Yap and concordant loss of expression of the Taz/Yap target genes, Ankrd1 and Cyr61, by qPCR was confirmed using pools or four individual siRNAs for each (Figures 1A and S1A–S1C). Knockdown efficiency was also verified by immunoblotting and immunofluorescence (IF) microscopy (Figures 1A and 1B), and the expected reduction of TGF-β-induced expression of Pai1 (Narimatsu et al., 2016) was also confirmed (Figure S1D). Density-induced polarization of epithelial cells can activate the Hippo pathway and leads to sequestration of Taz/Yap in the cytoplasm (Varelas et al., 2008; Narimatsu et al., 2015; Narimatsu et al., 2016); thus, as an alternative approach to remove Taz/Yap from the nucleus, varying concentrations of EpH4 cells were plated and Taz/Yap subcellular localization, protein levels, and phosphorylation were assessed. Immunofluorescence analysis confirmed that Taz/Yap localization to the cytoplasm increased with increasing cell density and a concordant, enhanced phosphorylation of Taz/Yap was observed at higher cell densities as monitored by immunoblotting

(Figures S2A and S2B). We confirmed that Smad phosphorylation was equivalent at all selected cell densities (Figure S2C), whereas density-dependent Hippo pathway activation was achieved as determined by analyzing the expression of the Taz/Yap target genes, Ankrd1 and Cyr61 by qPCR (Figure S2D). Prolonged treatment of polarized epithelial cells with TGF-β results in re-localization of the receptor to the basolateral surface (Narimatsu et al., 2015; Narimatsu et al., 2016). The equivalent levels of Smad phosphorylation observed (Figure S2C) indicate TGF-β receptor re-localization, which has been observed to occur at longer time points (Narimatsu et al., 2015), has not yet been manifested. To investigate the contribution of Taz/Yap to Smad function, we next monitored endogenous Smad nuclear accumulation in EpH4 cells transfected with control or Taz/Yap siRNAs using quantitative, automated high-content IF microscopy. In brief, cells were treated with varying doses of TGF-β for 0–3 h and after fixation, the distribution of Taz/Yap and Smads, as a ratio of the nuclear to cytoplasmic localization, in individual cells was quantitated by automated imaging (Figures 1C, S1E, and S1F). This method has the advantage that endogenous, rather than transfected and tagged, Smad2 is tracked and because efficient knockdown of Taz/Yap at the single cell level can be simultaneously monitored. Interestingly, analysis of the nuclear to cytoplasmic ratio of Smad2/3 revealed that the peak levels and the rate of Smad2/3 nuclear accumulation to this peak for all TGF-β doses tested were not notably altered when Taz/Yap was removed (Figure 1D). However, beyond this peak, the nuclear levels of Smad2/3 declined more rapidly in the absence of Taz/Yap. Similar results were observed in the case of the Smad2/3 partner, Smad4 (Figure 1E). These results suggest that removing Taz/Yap facilitates nuclear export of Smad2/3 and Smad4. Analysis of Smad nuclear accumulation at low and high cell densities confirmed that activating Hippo in response to increased cell density also reduces Smad nuclear accumulation (Figures S2E and S2F). Altogether, these observations indicate that Taz/Yap are involved in promoting Smad nuclear accumulation.

The Loss of Smad Nuclear Accumulation Caused by Loss of Taz/Yap Is Unlikely to Be due to Protein Degradation

Taz/Yap may alter Smad nuclear accumulation by acting as retention factors, by affecting phosphorylation/dephosphorylation and/or import rate of Smads, or by promoting degradation of Smads or TGF-β receptors. To assess whether loss of Smad nuclear accumulation is due to degradation of receptors or other proteins involved in the pathway, we first examined the expression levels of Smads in EpH4 cells transfected with siCTL or siTaz/Yap. Immunoblotting analysis revealed that no change in the levels of these proteins was observed during the signaling time period (Figure 2A). To check for the contribution of protein degradation in general, transfected EpH4 cells were treated with MG132, a reversible proteasome inhibitor that inhibits the degradation of ubiquitin-conjugated proteins. The results show that treating cells with MG132 caused a general increase in the accumulation of nuclear Smads; however, the difference between siCTL and siTaz/Yap at all doses of TGF-β was still observed (Figures 2B and 2C) indicating that the loss of Smad nuclear accumulation in siTaz/Yap transfected cells is unlikely to be due to degradation of Smads, Taz/Yap or TGF-β receptors.

Taz/Yap Knockdown Alters the Phosphorylation Status of Smads

We next investigated whether Taz/Yap knockdown affects phosphorylation or dephosphorylation of Smads. To do this, EpH4 cells were transfected with siCTL or siTaz/Yap and treated with two doses of TGF-β at varying time points. Immunoblotting experiments revealed that the initial rates of Smad phosphorylation are similar but that a more rapid decline in phosphorylation levels in cells transfected with siTaz/Yap, particularly at higher TGF-β doses, was observed (Figure 3). Dephosphorylation of Smads is thought to promote Smad nuclear export (ten Dijke and Hill, 2004; Xu, 2006); thus, these results are consistent with the IF experiments (Figure 1) that show constant Smad nuclear accumulation, up to the time of peak levels followed by a more rapid decrease in the levels of nuclear Smads upon the loss of Taz/Yap. These data also indicate that the initial levels of receptors are unaffected by loss of Taz/Yap.

Smad Nuclear Accumulation Is Not Altered in Cells Lacking Taz/Yap when TGF-β Receptors Are Inhibited by SB-431542

Our imaging results suggest that removing Taz/Yap facilitates Smad nuclear export. On the other hand, constitutive nucleocytoplasmic shuttling of Smads (Clarke et al., 2006) can allow for monitoring of receptor activity. To investigate if the increased loss of nuclear Smads induced by siTaz/Yap is due to changes in receptor activity, we inhibited TGF-β receptors by treating cells with SB-431542, an inhibitor of the TGF-β receptor type I (Inman et al., 2002). Analysis of the optimal timing and concentrations of SB-431542 to inhibit TGF-β receptors in EpH4 cells demonstrated that the compound was effective at 10 μM between 30 min

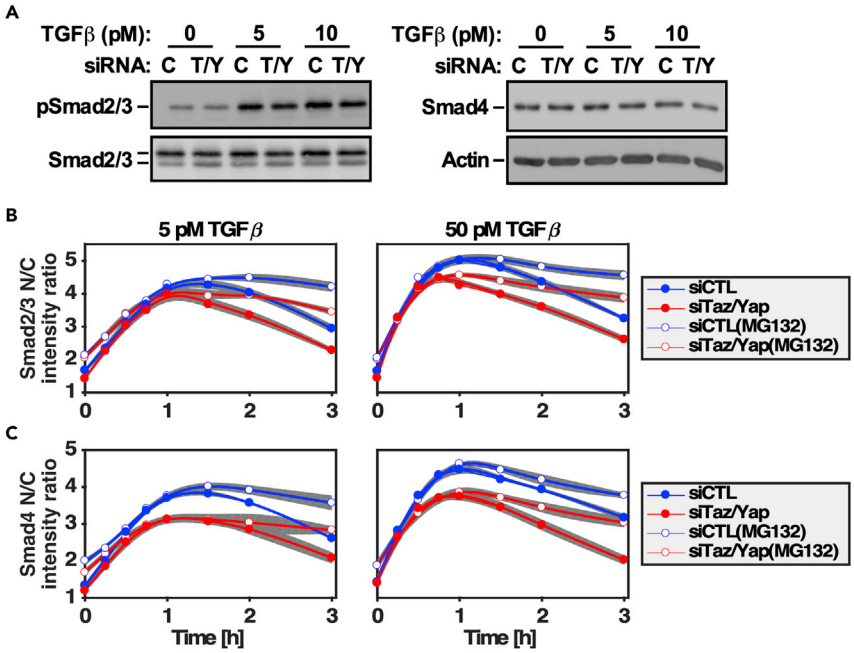

Figure 2. The Loss of Smad Nuclear Accumulation in siTaz/Yap-Transfected Cells Is Unlikely to Be due to Degradation of Smads/Taz/Yap Proteins or TGF-β Receptors

(A) EpH4 cells were transfected with siControl (C) or siTaz/Yap (T/Y) and then treated with 5 or 10 pM of TGF-β for 1.5 h. Immunoblotting shows that knockdown of Taz/Yap does not affect the expression level of Smads.

(B and C) EpH4 cells transfected with siControl (siCTL) or siTaz/Yap were seeded in a 96-well plate and treated with 10 μM of the proteasome inhibitor, MG132, both during the 3-h serum starvation time and during TGF-β treatment. The localization of Smad2/3 (B) and Smad4 (C) in response to 5 and 50 pM of TGF-β at varying time points was quantified for all cells/well by automated image analysis in five biological replicates. The full and empty circles show the mean, and the gray area indicates the mean ± standard error of the mean (SEM). The results show that MG132 treatment increases Smads accumulation but that the difference between siControl and siTaz/Yap still remains.

and up to 3 h of treatment (Figures S3A and S3B). Thus, EpH4 cells transfected with siCTL or siTaz/Yap were treated with TGF-β (5 and 50 pM) continuously or after 30 min of TGF-β addition; cells were washed to remove ligand and then incubated without (wash) or with 10 μM of SB-431542. Automated quantitation of the nuclear to cytoplasmic ratio of Smad2/3 and Smad4 confirmed that loss of Taz/Yap increased the apparent export rate of Smads (Figure 4) as in the previous IF experiments (Figure 1). However, this difference was lost when TGF-β receptors were inhibited (Figure 4). Thus, continuous TGF-β receptor activity is required for Taz/Yap-mediated effects on Smad nuclear accumulation to be manifested.

The Nuclear to Cytoplasmic Ratio of Taz/Yap Is Constant Regardless of Dose or Timing of TGF-β Treatment when Hippo Pathway Activity Is Unaltered

To determine the localization pattern of Taz/Yap during the time course of TGF-β treatment, EpH4 cells transfected with siCTL or siTaz/Yap were treated with different doses of TGF-β from 1 to 50 pM at varying times from 0 to 3 h and the nuclear to cytoplasmic ratio of Taz/Yap was quantified. The results showed noisy, but constant, signals (Figure S3C). The probability density of the nuclear to cytoplasmic ratios of Taz/Yap for cells transfected with siCTL or siTaz/Yap at different doses and time points (for approximately 10^5 cells) show that, for cells in either of the two conditions, the ratio (roughly 2.5) is similar (Figure S3D). We next used linear mixed-effects modeling to test the effects of multiple factors on the mean of the vector of ratios (Pinero and Bates, 2000; Gelman and Hill, 2006). This modeling revealed that the ratio was independent of TGF-β time and dose (see Transparent Methods and Table S1). Moreover, stepwise regression modeling (Hox et al., 2017) to determine which variables to include in the model yielded a Ratio ~1 + Id, where Id is the condition label, as the best model, thus also confirming that the ratio was independent of TGF-β (Table S2). We also experimentally confirmed that the nuclear to cytoplasmic ratio of Taz/Yap was independent of TGF-β treatment using subcellular fractionation followed by quantitation of immunoblots (Figure S3E). In contrast, the expected cell-density-induced cytoplasmic accumulation of Taz/Yap was

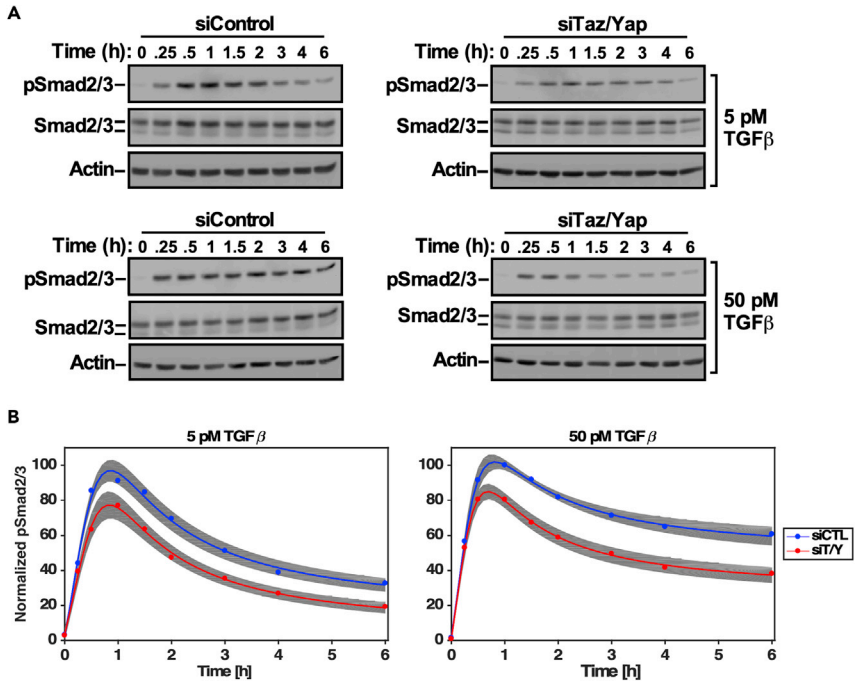

Figure 3. Taz/Yap Knockdown Alters Phosphorylation/Dephosphorylation of Smads

(A) EpH4 cells were transfected with siControl or siTaz/Yap and treated with two doses of TGF-β at varying times. A representative immunoblot is shown.

(B) Smad2/3 phosphorylation in seven different biological replicates was quantified by ImageJ software. The full circles show the mean, and the gray area indicates the mean ± the standard deviation of the different biological experiments.

readily detected using linear mixed-effects and stepwise regression modeling, whereas the time and dose of TGF-β did not have any influence on the Taz/Yap nuclear to cytoplasmic ratio (Figure S3F and Tables S3 and S4). Treating EpH4 cells with okadaic acid, a general phosphatase inhibitor that activates the Hippo pathway, (Hata et al., 2013) similarly reduced the ratio of nuclear to cytoplasmic of Taz/Yap (Figure S3G). Altogether, these results demonstrate that Taz/Yap localization is not altered by TGF-β and, thus, it is not necessary to consider changes in Taz/Yap localization in our modeling.

Mathematical Modeling of Smad Nuclear Accumulation Reveals Taz/Yap Is Not Involved in Nuclear Import of the Complex of pSmad2/3-Smad4

To compare nuclear import rates of the different forms of Smad complexes under control conditions, we turned to mathematical modeling. As Smads and Taz/Yap are sufficiently abundant, we selected a model using deterministic ordinary differential equations (ODE) based on the conservation of mass (Edelstein-Keshet, 2005). The proposed model contains binding of Taz/Yap to the complex of pSmad2/3-Smad4, the latter of which forms upon activation of the pathway by TGF-β addition (Figure 5 and Tables S5 and S6). To model the activated receptor, we used the impulse model (Chechik and Koller, 2009), a 7-parameter double-sigmoid function, one that captures activation and another that models destruction of functional TGF-β receptor complexes and post-translational mechanisms that provide negative feedback to the receptors that terminates signaling (Figure S4A). All other parameters are described in the Transparent Methods section and listed in Table S5.

Next, we set out to define the inputs and outputs of the process, which in our model corresponds to the dose of TGF-β and the nuclear accumulation of Smads, respectively. Signaling output is critically dependent on TGF-β dose and timing; thus, we experimentally determined sub-saturation doses. Examination of Smad phosphorylation in EpH4 cells treated with varying doses of TGF-β for different times revealed that doses of TGF-β below 20 pM avoids saturation of Smad phosphorylation and that a duration of 3 h captures the dynamics of the process (Figures 6A–6D). Of note, the saturation dose was unaltered by loss of Taz/Yap indicating that endogenous ligand levels are similar in both conditions (Figure 6B). As

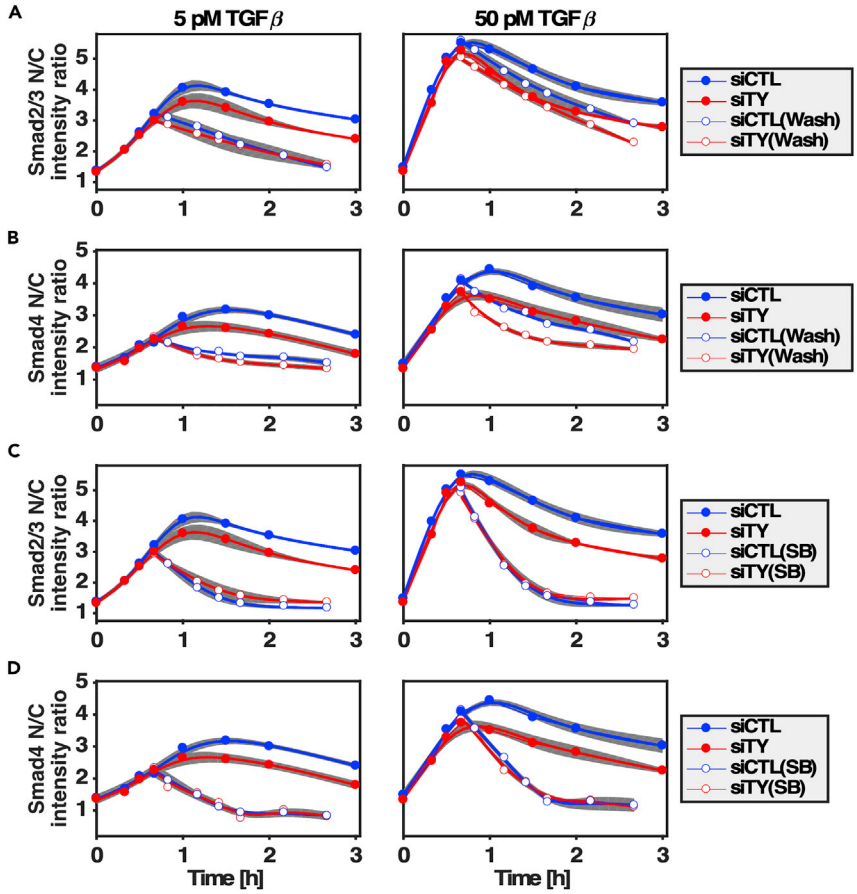

Figure 4. Altered Smad Nuclear Accumulation in the Absence of Taz/Yap Is Lost in the Presence of the TGF-β Receptor Inhibitor, SB-431542

EpH4 cells transfected with siCTL or siTaz/Yap (siT/Y) were treated with 5 or 50 pM TGF-β for the indicated times (full circles) or for 40 min after which TGF-β was washed out and fresh starvation media was added (A and B) or cells were incubated with 10 μM of SB-431542 for the indicated times (C and D; empty circles). All cells were simultaneously fixed, stained with DAPI, and Smads visualized using anti-Smad2/3 (A and C) or Smad4 (B and D) antibodies by immunofluorescence microscopy. The nuclear to cytoplasmic ratio of Smads was quantified by automated image analysis. The mean (full circles) ± standard error of the mean (SEM, gray area) from at least three independent biological experiments is shown.

our model requires the mass of Smad2/3, Smad4, and Taz/Yap, we converted the nuclear to cytoplasmic ratios obtained by immunofluorescence imaging into mass by taking into account the estimated volumes of the nucleus and cytoplasm (see Transparent Methods and Figures S4B–S4E).

The signaling process, as in most biological contexts, is characterized by uncertain parameters and noisy measurements. In this regard, the Markov chain Monte Carlo (MCMC) Differential Evolution Adaptive Metropolis (DREAM) technique is extremely useful for modeling (Vrugt et al., 2008a; Vrugt et al., 2009) and has been applied to variety of non-linear, high-dimensionality cases, including both environmental systems and biological contexts (Mitchener et al., 2015; Vrugt, 2016; Perry et al., 2019). Thus, to estimate the unknown parameters in the model, we used the MCMC DREAM$_{(ZS)}$ algorithm (Vrugt, 2016), which includes special extensions to simplify inference of high-dimensional and CPU-intensive system models and to minimize the number of samples required for burn-in (see Transparent Methods).

In the absence of stimulation, phosphorylated Smads and receptors are at non-zero, basal levels. To find the initial concentrations of the corresponding model species, we calculated their steady-state levels in the absence of TGF-β where the derivatives of concentrations of different proteins were equal to zero as reported by others (Strasen et al., 2018) (see Transparent Methods). At each iteration of the MCMC

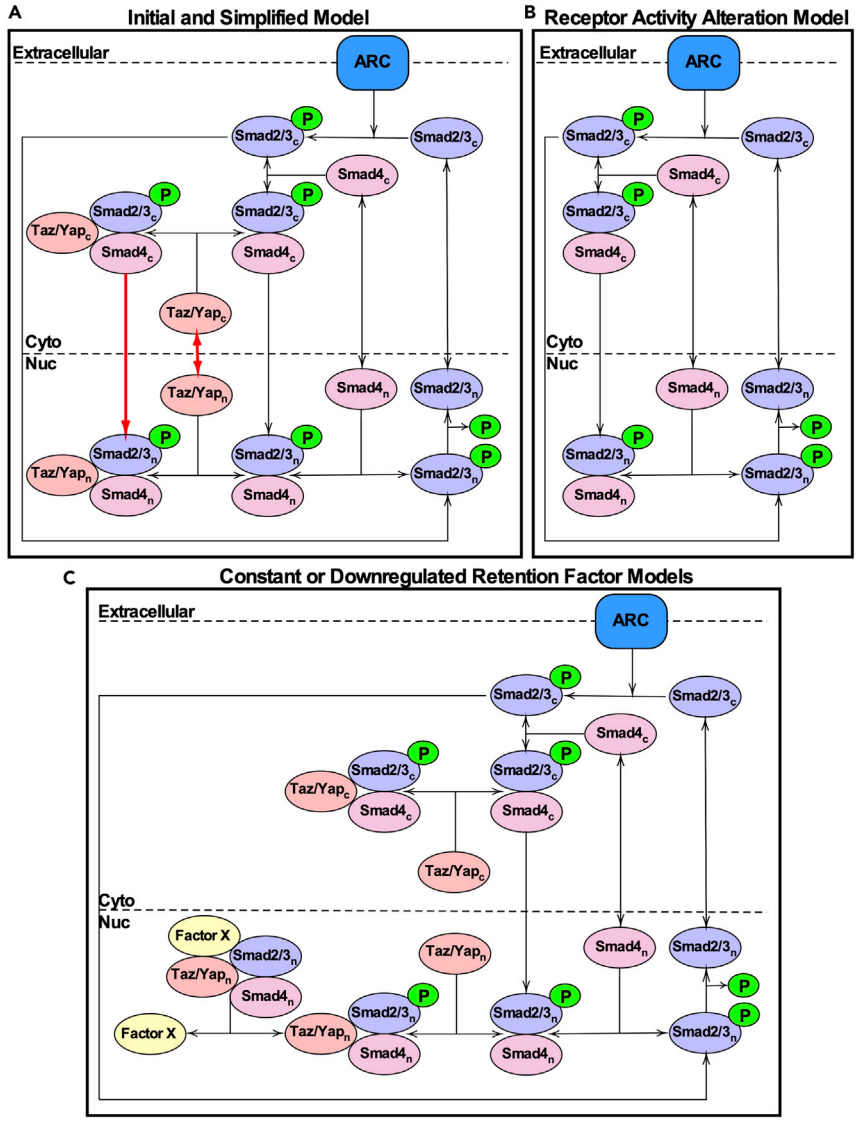

Figure 5. Models of TGF-β and Hippo Pathway Signaling Cross Talk

(A) The initial model contains binding of Taz/Yap to the complex of pSmad2/3-Smad4, which forms upon activation of the pathway by TGF-β addition. Since Taz/Yap localization is not altered by TGF-β and Taz/Yap is not involved in nucleocytoplasmic shuttling of the Smad complex, these steps (red arrows) are not considered in the simplified model.

(B) In the Receptor Activity Alteration (RAA) model, Taz/Yap still binds to the Smad complex; however, the binding has no effect on Smad nuclear accumulation, rather Taz/Yap alters receptor activity.

(C) In the Retention Factor (CRF or DRF) models there is a retention factor (X) in the nucleus, which binds to the complex of pSmad23-Smad4-Taz/Yap in a ligand-dependent manner. Factor X is either constant (Constant Retention Factor: CRF) or downregulated by the factor α, in the range [0 1] upon knocking down Taz/Yap (Downregulated Retention Factor: DRF).

DREAM$_{(ZS)}$ algorithm, the unknown initial values were estimated alongside with other unknown parameters of the model. To compare the import rates of the complexes pSmad2/3-Smad4 and pSmad2/3-Smad4-Taz/Yap, $k_{in-complex}$ and $k_{in-pSS4TY}$, we estimated the ratio, $\gamma = \frac{k_{in-pSS4TY}}{k_{in-complex}}$ alongside the other unknown model parameters for siCTL-transfected cells treated with three doses of TGF-β (2.5, 5, and 10 pM), selected for being below saturation, as well as in cells seeded at low or high cell densities and treated with 5 or 50 pM of TGF-β at different time points. The prior distribution for the ratio was selected in the range [0 5], which means that the import rate of the complex of pSmad2/3-Smad4-Taz/Yap can be up to five times more than the import rate of the pSmad2/3-Smad4 complex, which is a very conservative choice based on observed IF experiment results (Figures 1D and 1E). The estimated posterior distributions for the ratio,

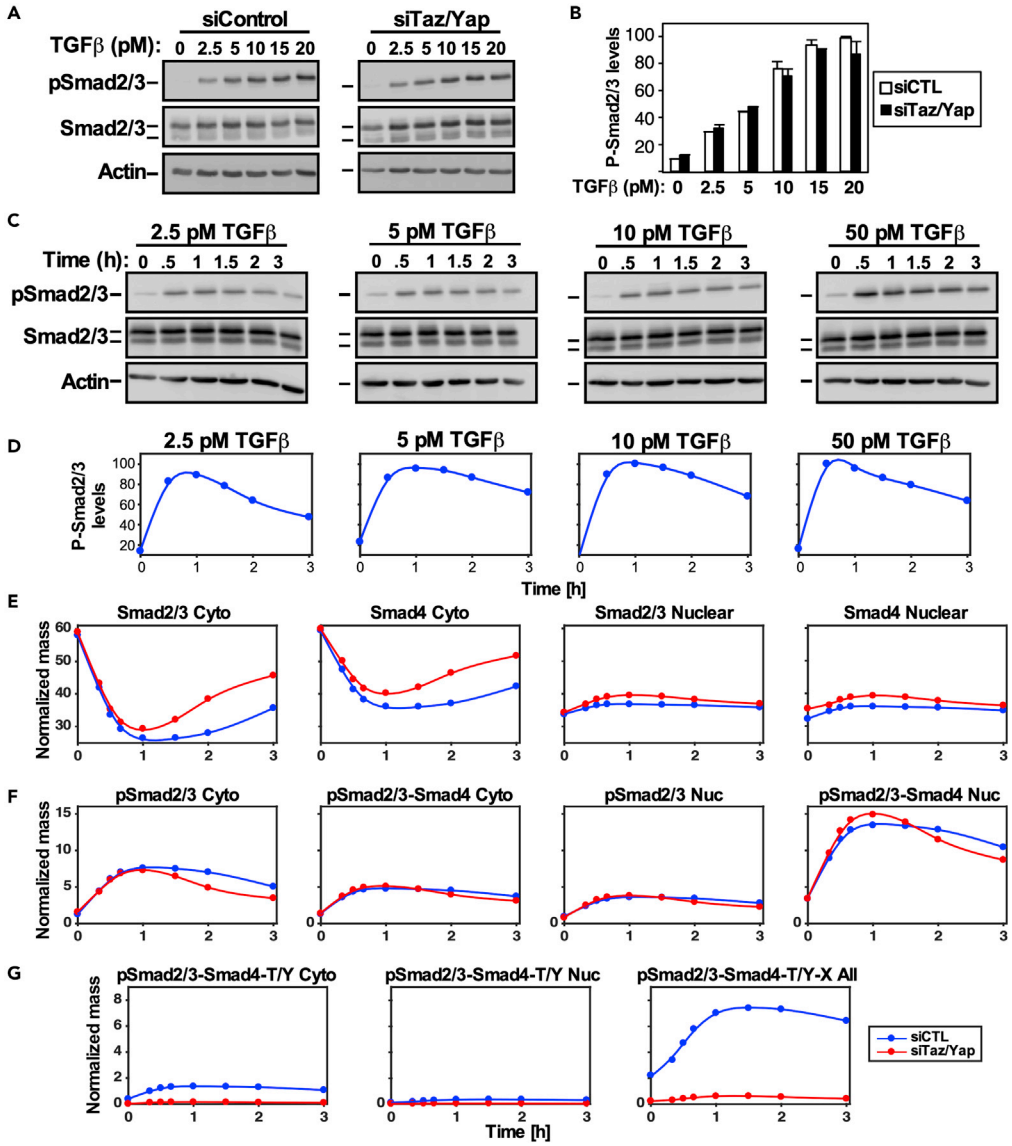

Figure 6. Determination of Below-Saturation TGF-β Doses for Model Input and Simulation of the Selected (RAADRF) Initial Model for Best Fitted Parameters

(A–D) Analysis of Smad phosphorylation in response to varying doses and times of TGF-β treatment. (A and B) EpH4 cells were transfected with siCTL or siTaz/Yap and treated with different doses of TGF-β for 30 min. (A) Smad phosphorylation was assessed by immunoblotting. (B) For quantitation, the intensity of each pSmad band was normalized to total Smad and then divided by the value of the sample with the highest pSmad levels (i.e., siCTL treated with 20 pM TGF-β) and was then multiplied by 100 to show percentage. Data, plotted as the mean ± standard deviation of four independent experiments, indicate that TGF-β doses below 20 pM should be used to avoid saturation of Smad phosphorylation. (C and D) EpH4 cells were plated at low density for 24 h and then were treated with TGF-β doses of 2.5, 5, 10, and 50 pM at varying time points. (C) Smad phosphorylation was assessed by immunoblotting. (D) Quantitation of Smad phosphorylation revealed the temporal patterns of signaling duration and allowed determination of the times of maximum phosphorylation for each dose of TGF-β, which occurred between 0.5 and 1 h. Simulation of the initial (RAADRF) selected model with the best fitted parameters.

(E) In cells transfected with siTaz/Yap, the concentration of free Smads in the cytoplasm or nucleus is higher than that of their counterparts in control cells.

(F) In siTaz/Yap transfected cells, cytoplasmic pSmad2/3 concentration is lower and there is no difference in pSmad2/3-Smad4 or nuclear pSmad2/3 as compared with controls. For nuclear pSmad2/3-Smad4, the mass is initially greater in siTaz/Yap than in control cells but then declines more rapidly, due to faster dephosphorylation.

Figure 6. *Continued*
(G) There is more pSmad2/3-Smad4-Taz/Yap in control cells than in cells transfected with siTaz/Yap in the cytoplasm, but no difference is observed in the nucleus for both conditions. Most of the complex in control cells is bound to the retention factor, X.

γ at the three aforementioned cases, shows that this rate is equal to zero and proposes that Taz/Yap has no role in the nuclear import of Smad complex (see Transparent Methods and Table S10). On the other hand, as the levels of Taz/Yap in the nucleus or cytoplasm, regardless of TGF-β treatment, are constant, then in the model,

$$\frac{d\left(\left[Taz/Yap_{Cyt}+pSmad.Smad4.Taz/Yap_{Cyt}\right]\right)}{dt}=\frac{d\left(\left[Taz/Yap_{Nuc}+pSmad.Smad4.Taz/Yap_{Nuc}\right]\right)}{dt}=0 \quad \text{(Equation 1)}$$

and

$$k_{in-TY}\left(k_{ex-TY}/k_{in-TY}\left[Taz/Yap_{Nuc}\right]-\left[Taz/Yap_{Cyt}\right]\right)=k_{in-pSS4TY}\left[pSmad.Smad4.Taz/Yap_{Cyt}\right]=0 \quad \text{(Equation 2)}$$

where k_{in-TY} and k_{ex-TY} are import and export rates of free (unbound) Taz/Yap, respectively. By assigning $k_{in-pSS4TY}=0$, free Taz/Yap either does not shuttle or shuttles between the nucleus and cytoplasm by a constant ratio, which is specified by Hippo pathway activity. However, the import and export rates of Taz/Yap are not identifiable using the current data. Since Taz/Yap is not involved in nucleocytoplasmic shuttling of the Smad complex, its shuttling is irrelevant to the model, and without a loss of generality, we used the simplified model (Figure 5A and Table S7).

To conduct identifiability analysis, which is a major challenge in biological reaction networks modeled by differential equations, we used the profile likelihood, a data-based method to detect structural and practical non-identifiability for reducing nonlinear models and to designate likely candidates for reduction (Raue et al., 2009; Maiwald et al., 2016). Confidence intervals, which contain the true value of the parameter with a desired probability, result in derivation of appropriate prior distributions for unknown parameters in the MCMC DREAM$_{(ZS)}$ algorithm. Identifiability analysis of the simplified model revealed that all the model parameters are structurally and practically identifiable as they have well-defined confidence intervals (Raue et al., 2009) (Figure S5A). The statistical analysis of the estimated parameters, the initial values for different cytoplasmic and nuclear complexes, and the parameter correlation matrix for the simplified model are given in Tables S11–S13. The goodness of fit test and the residual analysis (Figure S5Bi-iii) validated the model and confirmed that the data fit the model appropriately. Receptor activity for the best fitted (Maximum A Posteriori: MAP) parameter values reveal that the maximum activity occurs around 1.3 h and thereafter, owing to negative regulation, the receptor activity declines (Figure S5Biv). The 95% uncertainty ranges for the model simulation data due to parameter and total uncertainty confirms the model captured the process dynamics well (Figure S5Bv-viii).

Taz/Yap Knockdown May Reduce Nuclear Smad Accumulation by Both Altering TGF-β Receptor Activity and through a Retention Factor

To investigate if Taz/Yap knockdown changes receptor activity, acts as a retention factor, or both, we proposed three different hypotheses and established appropriate mathematical models to test the scenarios. First, to test if Taz/Yap knockdown alters TGF-β receptor activity and thus affects Smad phosphorylation and nuclear accumulation, the Receptor Activity Alteration (RAA) hypothesis, we used a model (Figure 5B and Table S8) in which Taz/Yap still binds to the Smad complex; however, the binding has no effect on Smad nuclear accumulation, rather Taz/Yap alters receptor activity. The parameters and initial values of different Smad complexes of the model were estimated simultaneously for siCTL or siTaz/Yap transfected cells treated with 10 pM TGF-β, a sub-saturation dose that still shows differential accumulation at the two conditions. Except for the receptors, all the other parameters were the same. Of note, these parameters were similar to those reported in HaCaT cells in a study examining TGF-β signaling alone (Schmierer et al., 2008). The statistical analysis of the estimated parameters, the initial values, and the parameter correlation matrix are given in Tables S14–S17. The estimated parameter values showed that all the receptor parameters h_0, h_1, h_2, t_1, β_1, and β_2 except t_2 (the offset time of the receptors) at the two conditions have the same probability distributions (Table S14). This observation suggests that a restricted model with all

parameters the same except the parameter t_2 at two conditions may explain the data. To test this, we estimated the restricted model parameters assuming that the six aforementioned parameters in the receptor models are the same (Tables S14–S17). The goodness of fit test, residual analysis, and time series plot of 95% simulation uncertainty ranges suggested that both models explain the data appropriately. Comparison of the temporal patterns of receptor activity for the MAP values for both models reveals that receptors for both conditions initially have the same activity; however, at around the peak, receptor activity in cells transfected with siTaz/Yap declines faster (Figures S6A–S6D and Table S15) consistent with results from IF and Smad phosphorylation (Figures 1 and 3). To discriminate the two proposed models, we used the Bayesian Model Averaging (BMA) strategy, which weighs the different models such that the weighted estimate (model) is a better predictor of the observed system behavior (data) than any of the individual models of the ensemble (Vrugt et al., 2008b). With BMA, the full model was rejected in favor of the restricted model, which means that the full model does not fit the data significantly better than the restricted model. Thus, we accepted the restricted model for RAA hypothesis.

A second mechanism to explain differential Smad nuclear accumulation is the retention-factor hypothesis, in which there are binding factors in the nucleus that have a higher affinity for phosphorylated Smads and thereby stabilize the complex of pSmad2/3-Smad4-Taz/Yap. To determine whether the presence of a nuclear retention factor could explain the differential Smad nuclear accumulation in cells transfected with siCTL or siTaz/Yap, we used a model (Figure 5C and Table S9) in which receptor activity parameters do not change but there is an unknown factor (X) in the nucleus, which binds to the complex of pSmad2/3-Smad4-Taz/Yap in a TGF-β-dependent manner. Although the factor could have a temporal pattern, we considered the simplest case where the concentration of X is constant during signaling. Two different scenarios were considered, X is either constant (Constant Retention Factor or CRF hypothesis) or downregulated by factor α, in the range [0 1] upon knocking down of Taz/Yap (Downregulated Retention Factor or DRF hypothesis). Statistical analysis of the estimated process parameters, initial values, and the parameter correlation matrices for the proposed models are summarized in Tables S18–S21. Validity of the models was confirmed by the residual analysis test and the chi-square goodness of fit (see Transparent Methods). The receptor activity in both models declines after 1 h. The 95% uncertainty ranges for the simulation data for the CRF and DRF models confirm that the measured data can be explained by both models (Figures S7A–S7D). Although both models fairly capture the process dynamics, applying the BMA strategy to discriminate the two proposed models (Vrugt et al., 2008b) rejected the DRF in favor of CRF. Simulation of the model for the best (MAP) parameters, using the initial values given in Table S18 at a dose of 10 pM TGF-β, so the role of the retention factor is manifested in a ligand-dependent manner shows that, until the peak, Smad nuclear accumulation is similar (Figure S7E) to the experimental results (see Figure 1). Altogether, our results show that existence a retention factor which protects the complex of pSmad in a ligand-dependent manner might be responsible for differential Smad nuclear accumulation.

Finally, to investigate whether both hypotheses may be valid, we used the same model but, in which both receptor parameters change and a nuclear retention factor exists, which is either constant, the Receptor Activity Alteration-Constant Retention Factor (RAACRF) hypothesis, or downregulated, the Receptor Activity Alteration-Downregulated Retention Factor (RAADRF) hypothesis, in cells lacking Taz/Yap. The parameters and initial values of both models were estimated (Tables S22 and S23) and there was no strong correlation between parameters (Tables S24 and S25). Validity of the models was confirmed by the residual analysis test, the chi-square goodness of fit test, and the 95% uncertainty ranges for the simulation data of both models (Figure S8). The receptor activity patterns at the two conditions show the same activity up to the peak, but this subsequently declines faster in cells transfected with siTaz/Yap (Figure S8). To discriminate the two proposed models, we used the BMA model selection strategy, which strongly rejected the RAACRF in favor of RAADRF.

So far, we have proposed and validated three different models to explain differential Smad nuclear accumulation in cells transfected with siCTL or siTaz/Yap. To compare to what extent the models fit the measured data, we used the BMA model selection strategy to find the best model among the three (Vrugt et al., 2008b). The estimated weights for the proposed models (Table S26) show that the RAA model is strongly rejected in favor of the other models, meaning that receptor activity alteration cannot be the sole factor responsible for differential nuclear accumulation. The RAADRF model was selected as the best model, whereas the Constant Retention Factor (CRF) model ranked between the two. The RAADRF model states that receptor activity will be reduced upon loss of Taz/Yap and that there is a

Taz/Yap-dependent nuclear retention factor that is downregulated in the absence of Taz/Yap. Simulating the identified model for the best (MAP) parameters showed that, upon phosphorylation, Smads translocate to the nucleus immediately (Figure 6E). In the nucleus, owing to the excess amount of Taz/Yap in control cells, the mass of the pSmad2/3-Smad4-Taz/Yap-X complex is roughly 10 times more than the complex si-Taz/Yap in transfected cells. This initially results in more, free, nuclear pSmad2/3-Smad4 in cells transfected with siTaz/Yap; however, after 1.5 h, this declines faster (Figures 6F and 6G).

The Mediator Complex Regulates Smad Nuclear Accumulation

Our mathematical modeling indicates that an unknown nuclear retention factor may explain differential Smad nuclear accumulation in cells lacking Taz/Yap. Candidate retention factors include transcriptional regulatory components such as the mediator complex, which is responsible for recruiting RNA polymerase to promoters (Soutourina, 2018) and which has been reported to associate with Taz/Yap (Varelas et al., 2008; Galli et al., 2015). In the RAADRF model, the expression of this retention factor is Taz/Yap regulated. Thus, we analyzed the expression of mediator complex components in transcriptomic data obtained by RNA sequencing from control versus siTaz/Yap-transfected cells. This revealed that, of the 30 mediator (Med) complex subunits expressed in EpH4 cells, only Med18 and Med12l showed a decrease in expression of approximately 2-fold. In agreement, analysis by qPCR demonstrated that expression of Med18 and Med12l mediator complex subunits were markedly decreased upon knocking down Taz/Yap either in the presence or absence of TGF-β (Figure 7A). Moreover, examination of TGF-β-induced Smad nuclear accumulation by IF revealed that knocking down Med18 decreased TGF-β-induced nuclear accumulation of both Smad2/3 and Smad4 (Figures 7B and 7C), although loss of Med12l had no affect (Figures 7D and 7E). The pattern of Smad accumulation in cells lacking Med18 is consistent with the IF and Smad phosphorylation results (Figures 1 and 3), with peak levels and the rate of Smad nuclear accumulation to this peak for both TGF-β doses being unaltered; but beyond the peak, the nuclear levels of Smads declined more rapidly in the absence of Med18. Of note, the effect was not as dramatic as that observed for siTaz/Yap, indicating besides regulating Med18, Taz/Yap can also modulate Smads via alternative means, such as regulating receptor activity as predicted in the RAADRF model.

DISCUSSION

TGF-β and Hippo pathway cross talk controls transcriptional outcomes, and key to TGF-β signaling is the nuclear localization of Smads. Thus, to investigate the role of the Hippo pathway mediators, Taz/Yap in Smad nuclear accumulation, we used experimental data and computational models of Hippo and TGF-β cross talk to test diverse hypotheses. Quantitative automated high-content IF microscopy showed that Taz/Yap enhances the nuclear accumulation of Smad2/3 and Smad4. Treating siTaz/Yap transfected EpH4 cells with MG132, a reversible proteasome inhibitor, showed the reduction in nuclear accumulation was not due to degradation of Smads, Taz/Yap proteins or receptors. On the other hand, immunoblotting and IF experiments revealed that Taz/Yap knockdown does not alter the initial rate of TGF-β-induced Smad phosphorylation or Smad nuclear accumulation to the peak, but rather resulted in a more rapid decrease from peak levels of both phospho-Smad and nuclear-localized Smads. Inhibiting TGF-β receptor activity by treating cells with SB-431542, an inhibitor of the TGF-β receptor type I, showed that the differential rate of Smad exit from the nucleus in siCTL versus siTaz/Yap transfected cells was lost, indicating that changes in receptor activity at the later stages of the process contributed to the effect of loss of Taz/Yap. In terms of Taz/Yap, high-throughput IF microscopy, immunoblotting, and statistical analysis showed that Taz/Yap levels in the cytoplasm or nucleus were constant regardless of dose of TGF-β or time of treatment as long as Hippo pathway activity was constant. Thus, to better understand the mechanism of the cross talk, we next developed several mathematical models to test different hypotheses. We selected appropriate doses of TGF-β and timing of treatment to acquire time course data for different complexes in the cytoplasm and nucleus. To estimate the unknown parameters in the models, we used the Bayesian method, MCMC DREAM$_{(ZS)}$ technique (Vrugt, 2016), which has been implemented to analyze a variety of scenarios involving nonlinearity, high dimensionality, and multimodality (Vrugt et al., 2008a; Vrugt et al., 2009). Initial applications were primarily in the weather and environmental fields, but the algorithm has also been used to model biochemical reactions such as COX2 and most recently to understand the role of a scaffolding protein in modulating MAPK activity (Mitchener et al., 2015; Vrugt, 2016; Perry et al., 2019). Here, we applied the approach to study signaling pathway cross talk. Identifying an initial mathematical model showed that Taz/Yap is not involved in nuclear import of the complex of pSmad2/3-Smad4, and so, the initial model was reduced to a simplified model, which does not consider the nuclear import of the complex pSmad2/3-Smad4-Taz/Yap or Taz/Yap shuttling. The profile likelihoods of parameters of the

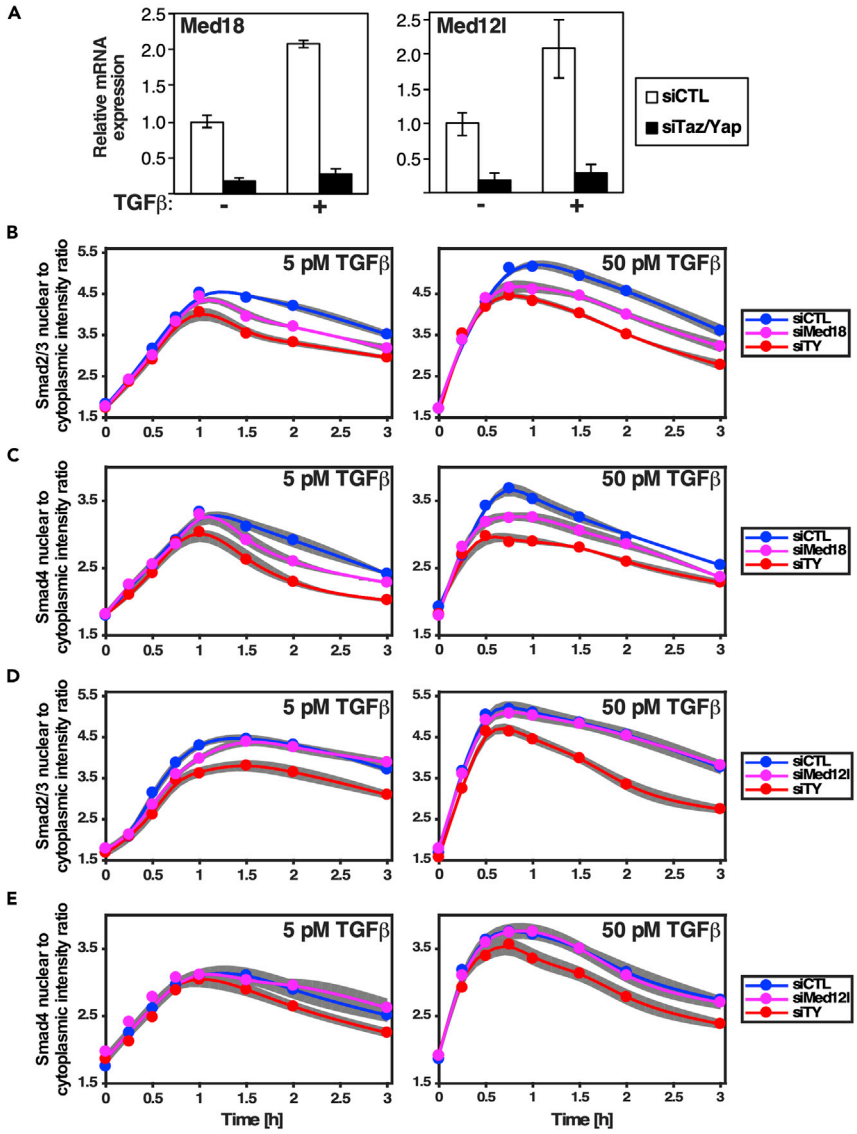

Figure 7. Mediator Complex Components Differentially Regulate Smad Nuclear Accumulation

(A) Analysis by qPCR shows that the mediator complex subunits, Med12l and Med18, are regulated by Taz/Yap. Data are shown as the mean ± standard deviation of three independent experiments.

(B–E) EpH4 cells were transfected with siCTL, siTaz/Yap, siMed18, or siMed12l and treated with two doses of TGF-β (5 and 50 pM) at different time points. Localization of Smad2/3 (B and D) and Smad4 (C and E) was quantified using automated IF imaging. (B and C) Loss of Med18, mediator complex subunit 18, diminishes nuclear accumulation of Smads. (D and E) Loss of Med12l has no effect on Smad accumulation. The full circles and gray areas indicate the mean ± standard error of the mean (SEM) of five biological replicates, respectively.

simplified model show that all the parameters of the model are identifiable and the model is not reducible. Based on the experimental data, modeling, and statistical analysis, several different hypotheses were proposed to explain differential accumulation of Smads, three of which (RAA, CRF, and RAADRF) captured the process dynamics appropriately. The Receptor Activity Alteration (RAA) hypothesis suggests that the differential nuclear accumulation of Smads is due to a decline of receptor activity that occurs earlier in cells lacking Taz/Yap. The retention-factor hypothesis states that there are binding factors in the nucleus, which have a higher affinity for phosphorylated Smads and stabilize the complex of pSmad2/3-Smad4-Taz/Yap. Mathematical modeling confirmed that a retention factor, in which the levels are not regulated by Taz/Yap (i.e., the CRF hypothesis), was an appropriate model. Finally, a combination model, RAADRF, which proposes that the differential accumulation of Smads at two conditions might be due to both receptor activity

alteration and existence of a Taz/Yap regulated retention factor also performed well. To compare to what extent these models fit the measured data, we used the BMA model selection strategy. While RAA was strongly rejected, CRF was ranked intermediately. The best model was determined to be RAADRF, that proposes that Taz/Yap is involved in receptor activity and that a nuclear Taz/Yap regulated retention factor, which stabilizes and protects the complex of Smad. Simulating the selected model shows there is more unphosphorylated Smads in both the cytoplasm and nucleus in Taz/Yap knocked down cells compared with the control. The concentration of pSmad2/3 in the cytoplasm is initially the same in siCTL and siTaz/Yap-transfected cells up to the peak but thereafter declines more rapidly in Taz/Yap-transfected cells. The concentration of nuclear pSmad2/3-Smad4 in siTaz/Tap cells is initially larger than controls owing to binding of this complex to Taz/Yap in control cells. However, it declines faster as the complex of pSmad2/3-Smad4 in control cells is protected by binding to Taz/Yap and subsequently to the factor X. Finally, roughly all of the nuclear pSmad2/3-Smad4-Taz/Yap in control cells is bound to the factor X. The simulation results confirm that receptor activity in Taz/Yap-transfected cells declines earlier and that the complex of pSmad2/3-Smad4 is protected by Taz/Yap and the factor, X. The RAADRF model was determined to be the best fit, but two proposed hypotheses (RAA and CRF) were not completely excluded. Applying the modeling approach we developed here in other cell lines may reveal that one of these alternate models would best fit the data in a different cell line. If so, this future work would have the potential to provide novel insights into context-dependent cross talk, a well-established characteristic of TGF-β signaling.

Our analysis indicated that differential TGF-β receptor activity upon loss of Taz/Yap may contribute to alterations in Smad nuclear accumulation. To date, phosphorylation, ubiquitination, SUMOylation, and N-linked glycosylation have been shown to modify the receptors post-translationally (Kim et al., 2012). Whether and how Taz/Yap may impact these events will require further investigation. Our results also predicted the existence of Taz/Yap-dependent retention factor(s). Candidate retention factors include transcription regulatory components or DNA-binding proteins. One such candidate is the mediator complex that is responsible for recruiting RNA polymerase to promoters and so affects maximum gene expression level (Soutourina, 2018). The mediator complex was reported to associate with Taz/Yap (Varelas et al., 2008; Galli et al., 2015). Our analysis revealed that the expression of Med18 and Med12l mediator complex subunits 18 and 12l were decreased upon knocking down Taz/Yap in EpH4 cells. Although Med12l had no effect on Smad nuclear accumulation, IF experiments confirmed that loss of Med18 reduced nuclear accumulation of both Smad2/3 and Smad4. However, as more dramatic effects were observed upon loss of Taz/Yap, the results indicate that other Taz/Yap-regulated factors such as other retention factors or receptor activity regulators are also likely be involved.

Limitations of the Study

Using the current data, the import and export rates of free Taz/Yap are not identifiable. However, as Taz/Yap is not involved in nucleocytoplasmic shuttling of the Smad complex, Taz/Yap shuttling is not relevant, and without a loss of generality, a simplified model was used. The nuclear retention factor could have a temporal pattern; however, based on available data, we only considered the simplest case in which the concentration of the retention factor is constant during signaling. Finally, an important factor that we were not able to directly investigate was the alteration of TGF-β receptor activity owing to the lack of availability of good receptor antibodies.

Resource Availability

Lead Contact

Further information and requests for resources should be directed to and will be fulfilled by the Lead Contact, Liliana Attisano (liliana.attisano@utoronto.ca).

Materials Availability

This study did not generate new unique materials.

Data and Code Availability

All data produced or analyzed for this study are included in the published article and its Supplemental Information files.

METHODS

All methods can be found in the accompanying Transparent Methods supplemental file.

SUPPLEMENTAL INFORMATION

Supplemental Information can be found online at https://doi.org/10.1016/j.isci.2020.101416.

ACKNOWLEDGMENTS

We thank Dr. J.A. Vrugt for advice on the implementation of DREAM MCMC. This work was supported by Canada First Research Excellence Fund/Medicine by Design and Canadian Institute for Health Research (CIHR) Foundation grants FDN148455 and FDN143252 to L.A. and J.L.W. B.L. held a CIHR studentship and L.A. and J.L.W. were CRC Chairs.

AUTHOR CONTRIBUTIONS

B.L. carried out experiments, developed the computational models, and wrote the manuscript. M.B. performed the imaging and developed the image analysis protocol. L.A. and J.L.W. supervised the study and wrote and edited the manuscript.

DECLARATION OF INTERESTS

The authors declare no competing interests.

Received: January 31, 2020
Revised: June 25, 2020
Accepted: July 27, 2020
Published: August 21, 2020

REFERENCES

Attisano, L., and Wrana, J.L. (2002). Signal transduction by the TGF-beta superfamily. Science *296*, 1646–1647.

Attisano, L., and Wrana, J.L. (2013). Signal integration in TGF-beta, WNT, and Hippo pathways. F1000Prime Rep. *5*, 17.

Barry, E.R., and Camargo, F.D. (2013). The Hippo superhighway: signaling crossroads converging on the Hippo/Yap pathway in stem cells and development. Curr. Opin. Cell Biol. *25*, 247–253.

Beyer, T.A., Narimatsu, M., Weiss, A., David, L., and Wrana, J.L. (2013). The TGFbeta superfamily in stem cell biology and early mammalian embryonic development. Biochim. Biophys. Acta *1830*, 2268–2279.

Budi, E.H., Duan, D., and Derynck, R. (2017). Transforming growth factor-beta receptors and Smads: regulatory Complexity and functional versatility. Trends Cell Biol. *27*, 658–672.

Chechik, G., and Koller, D. (2009). Timing of gene expression responses to environmental changes. J. Comput. Biol. *16*, 279–290.

Clarke, D.C., Betterton, M.D., and Liu, X. (2006). Systems theory of Smad signalling. Syst. Biol. (Stevenage) *153*, 412–424.

Clarke, D.C., and Liu, X. (2008). Decoding the quantitative nature of TGF-beta/Smad signaling. Trends Cell Biol. *18*, 430–442.

Craiu, R.V., and Rosenthal, J.S. (2014). Bayesian computation via Markov chain Monte Carlo. Annu. Rev. Stat. Appl. *1*, 179–201.

Edelstein-Keshet, L. (2005). Mathematical Models in Biology (SIAM). https://doi.org/10.1137/1.9780898719147.

Feng, X.H., and Derynck, R. (2005). Specificity and versatility in tgf-beta signaling through Smads. Annu. Rev. Cell Dev. Biol. *21*, 659–693.

Galli, G.G., Carrara, M., Yuan, W.C., Valdes-Quezada, C., Gurung, B., Pepe-Mooney, B., Zhang, T., Geeven, G., Gray, N.S., de Laat, W., et al. (2015). YAP drives growth by Controlling transcriptional pause release from dynamic enhancers. Mol. Cell *60*, 328–337.

Gelman, A., and Hill, J. (2006). Data Analysis Using Regression and Multilevel/hierarchical Models (Cambridge University Press).

Genevet, A., and Tapon, N. (2011). The Hippo pathway and apico-basal cell polarity. Biochem. J. *436*, 213–224.

Gurdon, J.B., and Bourillot, P.Y. (2001). Morphogen gradient interpretation. Nature *413*, 797–803.

Halder, G., and Johnson, R.L. (2011). Hippo signaling: growth control and beyond. Development *138*, 9–22.

Hata, A., and Chen, Y.-G. (2016). TGF-β signaling from receptors to Smads. Cold Spring Harb. Perspect. Biol. *8*, a022061.

Hata, Y., Timalsina, S., and Maimaiti, S. (2013). Okadaic Acid: a tool to study the hippo pathway. Mar. Drugs *11*, 896–902.

Hill, C.S. (2009). Nucleocytoplasmic shuttling of Smad proteins. Cell Res. *19*, 36–46.

Hill, C.S. (2016). Transcriptional control by the SMADs. Cold Spring Harb. Perspect. Biol. *8*, a022079.

Hoodless, P.A., Tsukazaki, T., Nishimatsu, S., Attisano, L., Wrana, J.L., and Thomsen, G.H. (1999). Dominant-negative Smad2 mutants inhibit activin/Vg1 signaling and disrupt axis formation in Xenopus. Dev. Biol. *207*, 364–379.

Hox, J.J., Moerbeek, M., and Van de Schoot, R. (2017). Multilevel Analysis: Techniques and Applications (Routledge).

Inman, G.J., Nicolas, F.J., Callahan, J.F., Harling, J.D., Gaster, L.M., Reith, A.D., Laping, N.J., and Hill, C.S. (2002). SB-431542 is a potent and specific inhibitor of transforming growth factor-beta superfamily type I activin receptor-like kinase (ALK) receptors ALK4, ALK5, and ALK7. Mol. Pharmacol. *62*, 65–74.

Kang, Y., Chen, C.-R., and Massagué, J. (2003). A self-enabling TGF-β response coupled to stress signaling: Smad engages stress response factor ATF3 for Id1 repression in epithelial cells. Mol. Cell *11*, 915–926.

Kim, Y.-W., Park, J., Lee, H.-J., Lee, S.-Y., and Kim, S.-J. (2012). TGF-β sensitivity is determined by N-linked glycosylation of the type II TGF-β receptor. Biochem. J. *445*, 403–411.

Kirk, P., Silk, D., and Stumpf, M.P. (2016). Reverse engineering under uncertainty. In Uncertainty in Biology, L. Geris and D. Gomez-Cabrero, eds. (Springer), pp. 15–32.

Ma, S., Meng, Z., Chen, R., and Guan, K.-L. (2019). The Hippo pathway: biology and pathophysiology. Annu. Rev. Biochem. *88*, 577–604.

Maiwald, T., Hass, H., Steiert, B., Vanlier, J., Engesser, R., Raue, A., Kipkeew, F., Bock, H.H., Kaschek, D., Kreutz, C., and Timmer, J. (2016). Driving the model to its limit: profile likelihood based model reduction. PLoS One *11*, e0162366.

Mauviel, A., Nallet-Staub, F., and Varelas, X. (2012). Integrating developmental signals: a Hippo in the (path) way. Oncogene *31*, 1743.

McNeill, H., and Woodgett, J.R. (2010). When pathways collide: collaboration and connivance among signalling proteins in development. Nat. Rev. Mol. Cell Biol. *11*, 404–413.

Misra, J.R., and Irvine, K.D. (2018). The Hippo signaling network and its biological functions. Annu. Rev. Genet. *52*, 65–87.

Mitchener, M.M., Hermanson, D.J., Shockley, E.M., Brown, H.A., Lindsley, C.W., Reese, J., Rouzer, C.A., Lopez, C.F., and Marnett, L.J. (2015). Competition and allostery govern substrate selectivity of cyclooxygenase-2. Proc. Natl. Acad. Sci. U S A *112*, 12366–12371.

Narimatsu, M., Labibi, B., Wrana, J.L., and Attisano, L. (2016). Analysis of Hippo and TGFbeta signaling in polarizing epithelial cells and mouse embryos. Differentiation *91*, 109–118.

Narimatsu, M., Samavarchi-Tehrani, P., Varelas, X., and Wrana, J.L. (2015). Distinct polarity cues direct Taz/Yap and TGFbeta receptor localization to differentially control TGFbeta-induced Smad signaling. Dev. Cell *32*, 652–656.

Nicolás, F.J., De Bosscher, K., Schmierer, B., and Hill, C.S. (2004). Analysis of Smad nucleocytoplasmic shuttling in living cells. J. Cell Sci. *117*, 4113–4125.

Park, H.W., and Guan, K.L. (2013). Regulation of the Hippo pathway and implications for anticancer drug development. Trends Pharmacol. Sci. *34*, 581–589.

Perry, N.A., Kaoud, T.S., Ortega, O.O., Kaya, A.I., Marcus, D.J., Pleinis, J.M., Berndt, S., Chen, Q., Zhan, X., Dalby, K.N., et al. (2019). Arrestin-3 scaffolding of the JNK3 cascade suggests a mechanism for signal amplification. Proc. Natl. Acad. Sci. U S A *116*, 810–815.

Pinero, J., and Bates, D. (2000). Mixed-effects Models in S and S-PLUS (Statistics and Computing) (Springer).

Raue, A., Kreutz, C., Maiwald, T., Bachmann, J., Schilling, M., Klingmuller, U., and Timmer, J. (2009). Structural and practical identifiability analysis of partially observed dynamical models by exploiting the profile likelihood. Bioinformatics *25*, 1923–1929.

Schmierer, B., and Hill, C.S. (2005). Kinetic analysis of Smad nucleocytoplasmic shuttling reveals a mechanism for transforming growth factor beta-dependent nuclear accumulation of Smads. Mol. Cell. Biol. *25*, 9845–9858.

Schmierer, B., and Hill, C.S. (2007). TGFbeta-SMAD signal transduction: molecular specificity and functional flexibility. Nat. Rev. Mol. Cell Biol. *8*, 970–982.

Schmierer, B., Tournier, A.L., Bates, P.A., and Hill, C.S. (2008). Mathematical modeling identifies Smad nucleocytoplasmic shuttling as a dynamic signal-interpreting system. Proc. Natl. Acad. Sci. U S A *105*, 6608–6613.

Shi, Y., and Massague, J. (2003). Mechanisms of TGF-beta signaling from cell membrane to the nucleus. Cell *113*, 685–700.

Soutourina, J. (2018). Transcription regulation by the Mediator complex. Nat. Rev. Mol. Cell Biol. *19*, 262.

Strasen, J., Sarma, U., Jentsch, M., Bohn, S., Sheng, C., Horbelt, D., Knaus, P., Legewie, S., and Loewer, A. (2018). Cell-specific responses to the cytokine TGFbeta are determined by variability in protein levels. Mol. Syst. Biol. *14*, e7733.

Stuart, A.M. (2010). Inverse problems: a Bayesian perspective. Acta Numer. *19*, 451–559.

ten Dijke, P., and Hill, C.S. (2004). New insights into TGF-beta-Smad signalling. Trends Biochem. Sci. *29*, 265–273.

Varelas, X., Sakuma, R., Samavarchi-Tehrani, P., Peerani, R., Rao, B.M., Dembowy, J., Yaffe, M.B., Zandstra, P.W., and Wrana, J.L. (2008). TAZ controls Smad nucleocytoplasmic shuttling and regulates human embryonic stem-cell self-renewal. Nat. Cell Biol. *10*, 837–848.

Varelas, X., Samavarchi-Tehrani, P., Narimatsu, M., Weiss, A., Cockburn, K., Larsen, B.G., Rossant, J., and Wrana, J.L. (2010). The Crumbs complex couples cell density sensing to Hippo-dependent control of the TGF-beta-SMAD pathway. Dev. Cell *19*, 831–844.

Villaverde, A.F., and Banga, J.R. (2014). Reverse engineering and identification in systems biology: strategies, perspectives and challenges. J. R. Soc. Interface *11*, 20130505.

Vrugt, J.A. (2016). Markov chain Monte Carlo simulation using the DREAM software package: theory, concepts, and MATLAB implementation. Environ. Model. Softw. *75*, 273–316.

Vrugt, J.A., Ter Braak, C.J., Clark, M.P., Hyman, J.M., and Robinson, B.A. (2008a). Treatment of input uncertainty in hydrologic modeling: doing hydrology backward with Markov chain Monte Carlo simulation. Water Resour. Res. *44*, https://doi.org/10.1029/2007WR006720.

Vrugt, J.A., Diks, C.G., and Clark, M.P. (2008b). Ensemble Bayesian model averaging using Markov chain Monte Carlo sampling. Environ. Fluid Mech. *8*, 579–595.

Vrugt, J.A., Ter Braak, C., Diks, C., Robinson, B.A., Hyman, J.M., and Higdon, D. (2009). Accelerating Markov chain Monte Carlo simulation by differential evolution with self-adaptive randomized subspace sampling. Int. J. Nonlin. Sci. Num. Simulat. *10*, 273–290.

Xu, L. (2006). Regulation of Smad activities. Biochim. Biophys. Acta *1759*, 503–513.

Xu, L., Kang, Y., Çöl, S., and Massagué, J. (2002). Smad2 nucleocytoplasmic shuttling by nucleoporins CAN/Nup214 and Nup153 feeds TGF-β signaling complexes in the cytoplasm and nucleus. Mol. Cell *10*, 271–282.

Yu, F.X., Zhao, B., and Guan, K.L. (2015). Hippo pathway in organ size control, tissue homeostasis, and cancer. Cell *163*, 811–828.

Zi, Z., Feng, Z., Chapnick, D.A., Dahl, M., Deng, D., Klipp, E., Moustakas, A., and Liu, X. (2011). Quantitative analysis of transient and sustained transforming growth factor-β signaling dynamics. Mol. Syst. Biol. *7*, 492.

Zi, Z., and Klipp, E. (2007). Constraint-based modeling and kinetic analysis of the Smad dependent TGF-β signaling pathway. PLoS One *2*, e936.

iScience, Volume *23*

Supplemental Information

Modeling the Control of TGF-β/Smad Nuclear Accumulation by the Hippo Pathway Effectors, Taz/Yap

Bita Labibi, Mikhail Bashkurov, Jeffrey L. Wrana, and Liliana Attisano

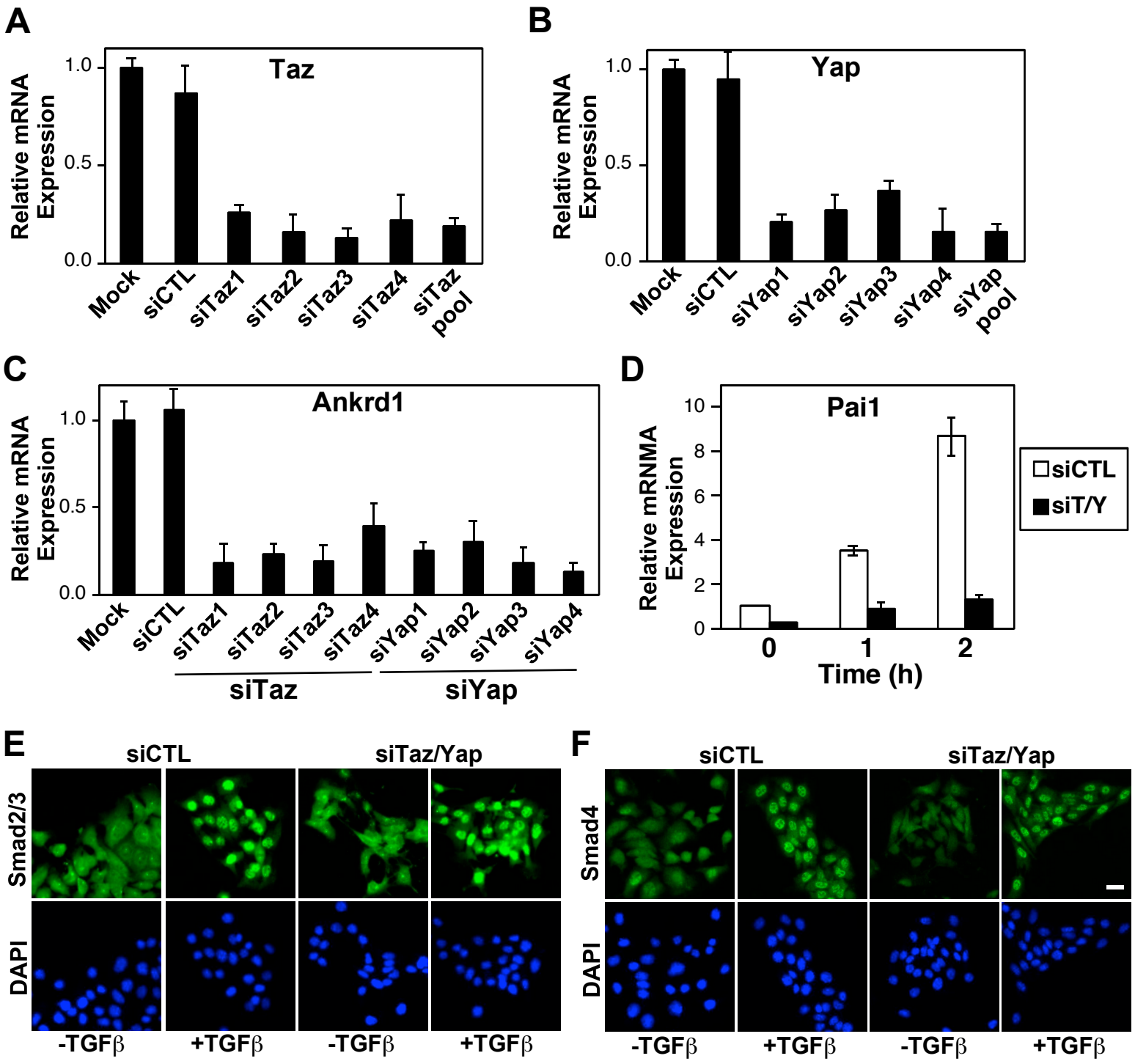

Figure S1. Knockdown of Taz and Yap attenuates expression of Hippo and TGFβ target genes (related to Figure 1).

(**A-C**) Expression of Taz and Yap and the Hippo target gene, Ankrd1, upon knockdown using single and pools of siTaz and siYAP was determined by qPCR. Data is plotted as the mean +/- standard deviation of a representative experiment. (**D**) Analysis of Pai1 expression in EpH4 cells transfected with siCTL or siTaz/Yap pools and treated with 10 pM TGFβ for the indicated times was determined by qPCR. Data is shown as the mean +/- standard deviation of six different biological experiments. (**E, F**) EpH4 cells were transfected with siCTL or siTaz/Yap and then treated with 5 pM TGFβ for 1 hr. Cells were fixed, nuclei visualized with DAPI and Smad proteins stained with antibodies against (**E**) Smad2/3 or (**F**) Smad4 and representative images, visualized using an IN Cell Analyzer 6000, are shown. Scale bar, 200 μm.

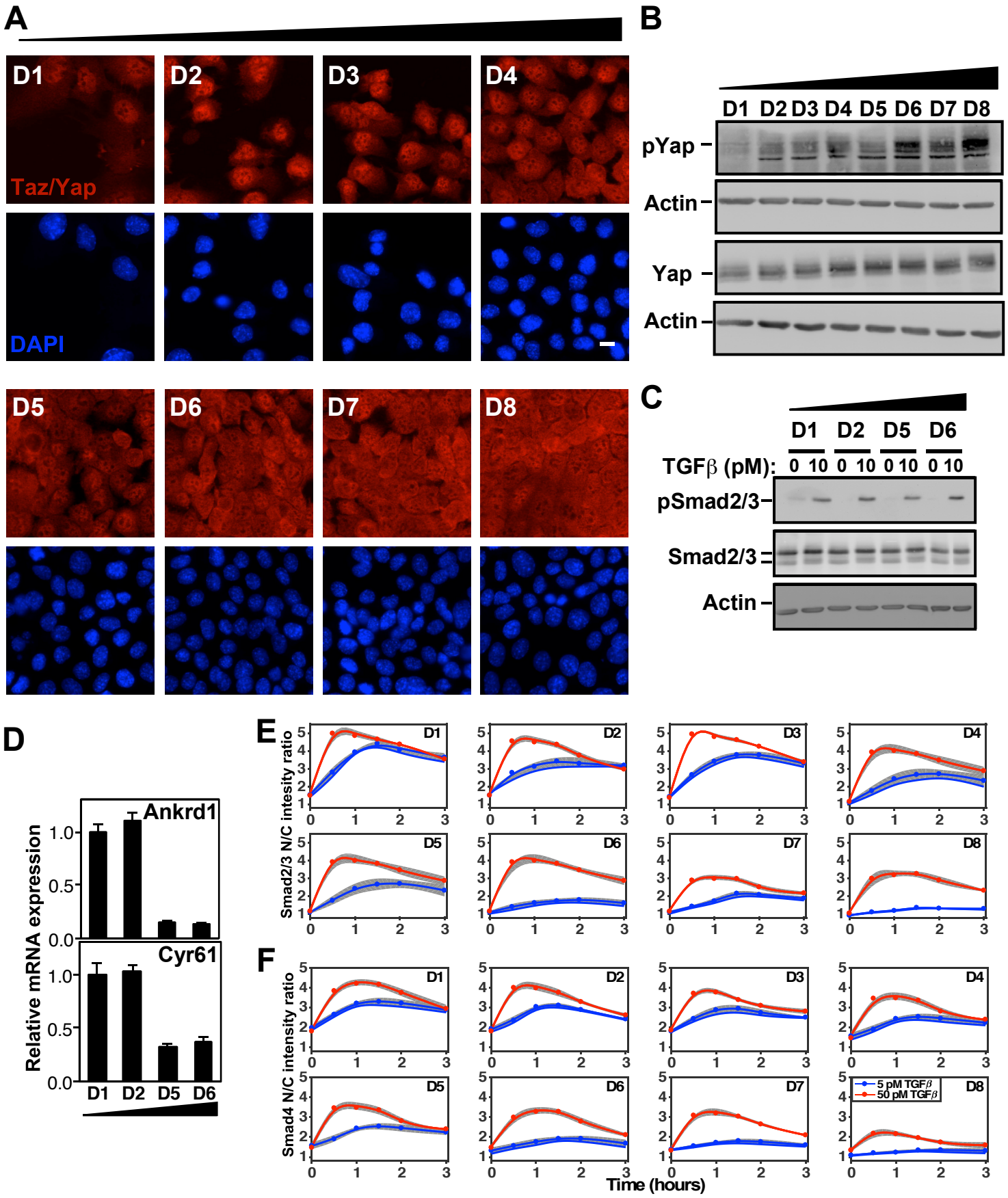
A
D1
D2
D3
D4
Taz/Yap
DAPI
D5
D6
D7
D8
B
D1 D2 D3 D4 D5 D6 D7 D8
pYap
Actin
Yap
Actin
C
D1 D2 D5 D6
TGFβ (pM): 0 10 0 10 0 10 0 10
pSmad2/3
Smad2/3
Actin
D
Ankrd1
Cyr61
Relative mRNA expression
1.0
0.5
0.0
D1 D2 D5 D6
E
Smad2/3 N/C intesity ratio
F
Smad4 N/C intensity ratio
Time (hours)
5 pM TGFβ
50 pM TGFβ

Figure S2

Figure S2. The Hippo pathway is activated in response to increasing cell density (related to Figure 1). (**A**) EpH4 cells were seeded at 8 different cell densities (D) (D1: $5x10^3$, D2: $8x10^3$, D3: $10x10^3$, D4: $20x10^3$, D5: $40x10^3$, D6: $60x10^3$, D7: $80x10^3$, D8: $100x10^3$ cells/cm^2) in a 96-well plate for 24 h. The localization of Taz/Yap in cells co-stained with DAPI was determined by immunofluorescence microscopy. Representative images of cells are shown. Scale = 100 μM. (**B**) EpH4 cells were seeded at 8 different cell densities (as above) in a 6-well plate for 24 h. Yap phosphorylation levels were determined by immunoblotting using the indicated antibodies. (**C**) EpH4 cells were seeded at 4 cell densities (as above) and after 24 h were treated with 10 pM of TGFβ for 30 min. Smad phosphorylation was assessed by immunoblotting using the indicated antibodies. Note that there is no change in Smad2/3 phosphorylation at any cell density. (**D**) Density dependent activation of the Hippo pathway was confirmed by analyzing the expression of Taz/Yap target genes, Ankrd1 and Cyr61 by qPCR. Data is shown as the mean +/- standard deviation of 3 independent experiments. (**E, F**) EpH4 cells were seeded at 8 different cell densities (as in A) were starved with 0.1% serum-containing media for 3 h and then treated with 5 and 50 pM TGFβ at different time points. Cells were fixed, nuclei visualized with DAPI and Smad proteins stained with antibodies against (**E**) Smad2/3 or (**F**) Smad4 and visualized by IF. Images were taken by confocal microscopy using IN Cell Analyzer 6000. Smad protein localization of ~1000 cells/well in six biological replicates was quantified by automated image analysis and is plotted as the mean (full circles) +/- standard error of the mean (SEM, gray area).

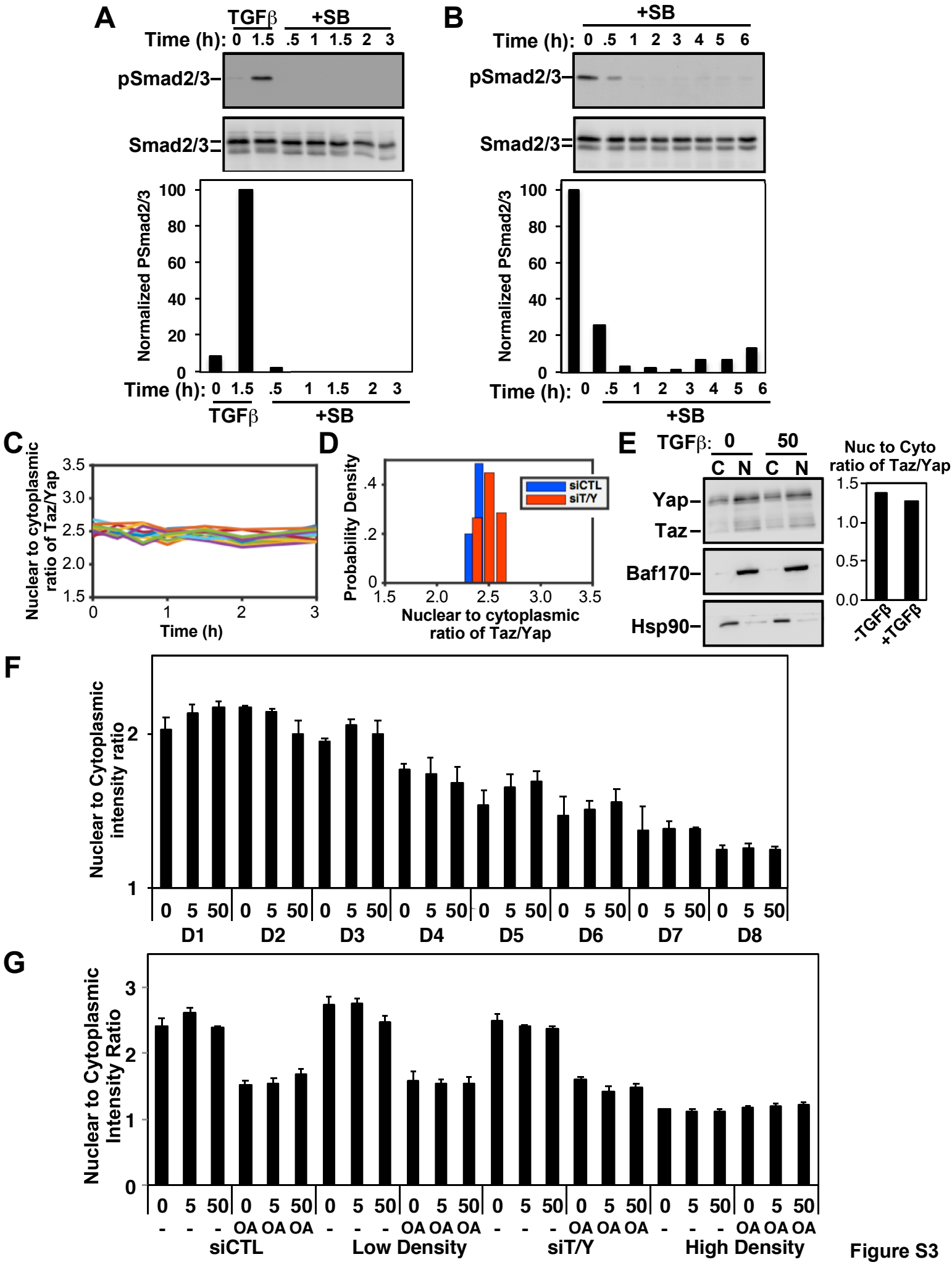
A
TGFβ
+SB
Time (h): 0 1.5 .5 1 1.5 2 3
pSmad2/3
Smad2/3
Normalized PSmad2/3
100
80
60
40
20
0
Time (h): 0 1.5 .5 1 1.5 2 3
TGFβ
+SB
B
+SB
Time (h): 0 .5 1 2 3 4 5 6
pSmad2/3
Smad2/3
Normalized PSmad2/3
100
80
60
40
20
0
Time (h): 0 .5 1 2 3 4 5 6
+SB
C
Nuclear to cytoplasmic ratio of Taz/Yap
3.5
3.0
2.5
2.0
1.5
0
1
2
3
Time (h)
D
Probability Density
.4
.2
0
siCTL
siT/Y
1.5
2.0
2.5
3.0
3.5
Nuclear to cytoplasmic ratio of Taz/Yap
E
TGFβ: 0 50
C N C N
Yap
Taz
Baf170
Hsp90
Nuc to Cyto ratio of Taz/Yap
1.5
1.0
0.5
0.0
-TGFβ
+TGFβ
F
Nuclear to Cytoplasmic intensity ratio
2
1
0 5 50 0 5 50 0 5 50 0 5 50 0 5 50 0 5 50 0 5 50 0 5 50
D1 D2 D3 D4 D5 D6 D7 D8
G
Nuclear to Cytoplasmic Intensity Ratio
3
2
1
0
0 5 50 0 5 50 0 5 50 0 5 50 0 5 50 0 5 50 0 5 50 0 5 50
- - - OA OA OA - - - OA OA OA - - - OA OA OA - - - OA OA OA
siCTL
Low Density
siT/Y
High Density

Figure S3

Figure S3: Evaluating the effect of TGFβ signalling on phosphorylation of Smad2/3 and localization of Taz/Yap (related to Figures 4 and 5).

(**A, B**) Evaluating the effect of SB-431542 on phosphorylation of Smad2/3. EpH4 cells transfected with siCTL or siTaz/Yap were treated with 10 pM of TGFβ for 1.5 h (**A**) or 10 μM of SB-431542 drug (**A, B**) for the indicated times. Quantitation of immunoblots shows efficient inhibition of Smad phosphorylation in response to drug treatment for up to 3 h, after which phosphorylation resumes due to short lifetime of SB-431542. (**C**) The nuclear to cytoplasmic ratio of Taz/Yap is constant regardless of dose or timing of TGFβ treatment when Hippo pathway activity is constant. The ratio of nuclear to cytoplasmic intensities of Taz/Yap in one representative experiment of cells transfected with siCTL or siTaz/Yap and treated with different doses of TGFβ (1, 2.5, 5, 10, 20 and 50 pM) at different time points for at least 10^5 cells per experiment as in Figure 1 was quantified by automatic imaging. The plot shows that the ratio is a noisy constant signal. (**D**) The probability densities of the ratios for cells transfected with siCTL or siTaz/Yap are similar. (**E**) EpH4 cells were seeded at low cell density and treated with 50 pM of TGFβ for 1 h. Cells were subjected to nuclear (N)/cytoplasmic (C) fractionation followed by immunoblotting for TazYap and the cytoplasmic and nuclear compartment markers, Hsp90 and Baf170, respectively. Quantification by ImageJ software shows that the nuclear to cytoplasmic ratios of Taz/Yap are independent of the dose of TGFβ. (**F**) EpH4 cells were seeded at different cell densities (D1-D8), as in Figure S1 in a 96-well plate and treated with 5 or 50 pM doses of TGFβ at varying times. Quantification of the nuclear to cytoplasmic ratio of Taz/Yap reveals that the ratio changes by Hippo pathway activation in response to cell density. (**G**) EpH4 cells were transfected with siCTL or siTaz/Yap, seeded at low or high cell densities, treated with 5 or 50 pM of TGFβ at varying time points in presence or absence of okadaic acid (OA) in a 96-well plate and the nuclear to cytoplasmic ratio of Taz/Yap was quantified. The results show that the ratio changes by activating the Hippo pathway either by increasing cell density or by treating with okadaic acid.

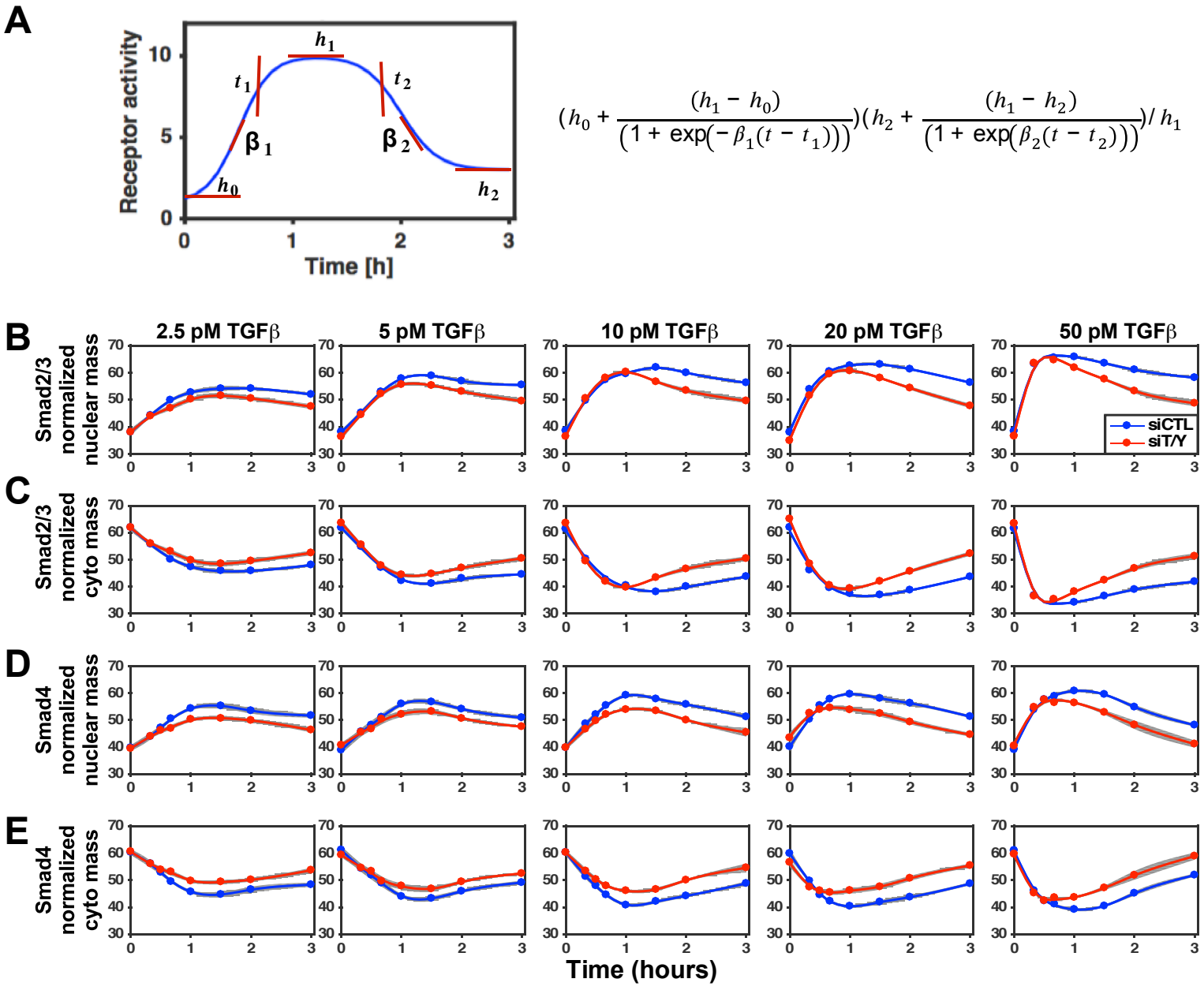

Figure S4. Establishing the initial model of TGFβ and Hippo pathways signaling crosstalk (related to Figures 1 and 5).

(**A**) The impulse model was used to model the activated receptor. In the impulse model, a 7-parameter-sigmoid function, one that captures activation, and another that models destruction of functional TGFβ receptor complexes was used. The impulse model models temporal responses with an onset followed by an offset transition to a steady state response. The model function has three amplitude (height) parameters, the initial amplitude, h_0, the peak amplitude, h_1, and the steady state amplitude, h_2, the onset time, t_1, the offset time, t_2 and the slope parameters, β_1 and β_2. (**B-D**) Normalized nuclear and cytoplasmic concentrations of Smad2/3 and Smad4 upon loss of Taz/YAP expression. The nuclear to cytoplasmic ratios obtained by IF imaging were converted into normalized mass by taking into account the volume of the nucleus and cytoplasm. The mean (full circles) +/- standard error of the mean (SEM, gray area) from at least nine independent biological experiments is shown. (**B**) Normalized mass of nuclear Smad2/3, (**C**) Normalized mass of cytoplasmic Smad2/3, (**D**) Normalized mass of nuclear Smad4 and (E) Normalized mass of cytoplasmic Smad4.

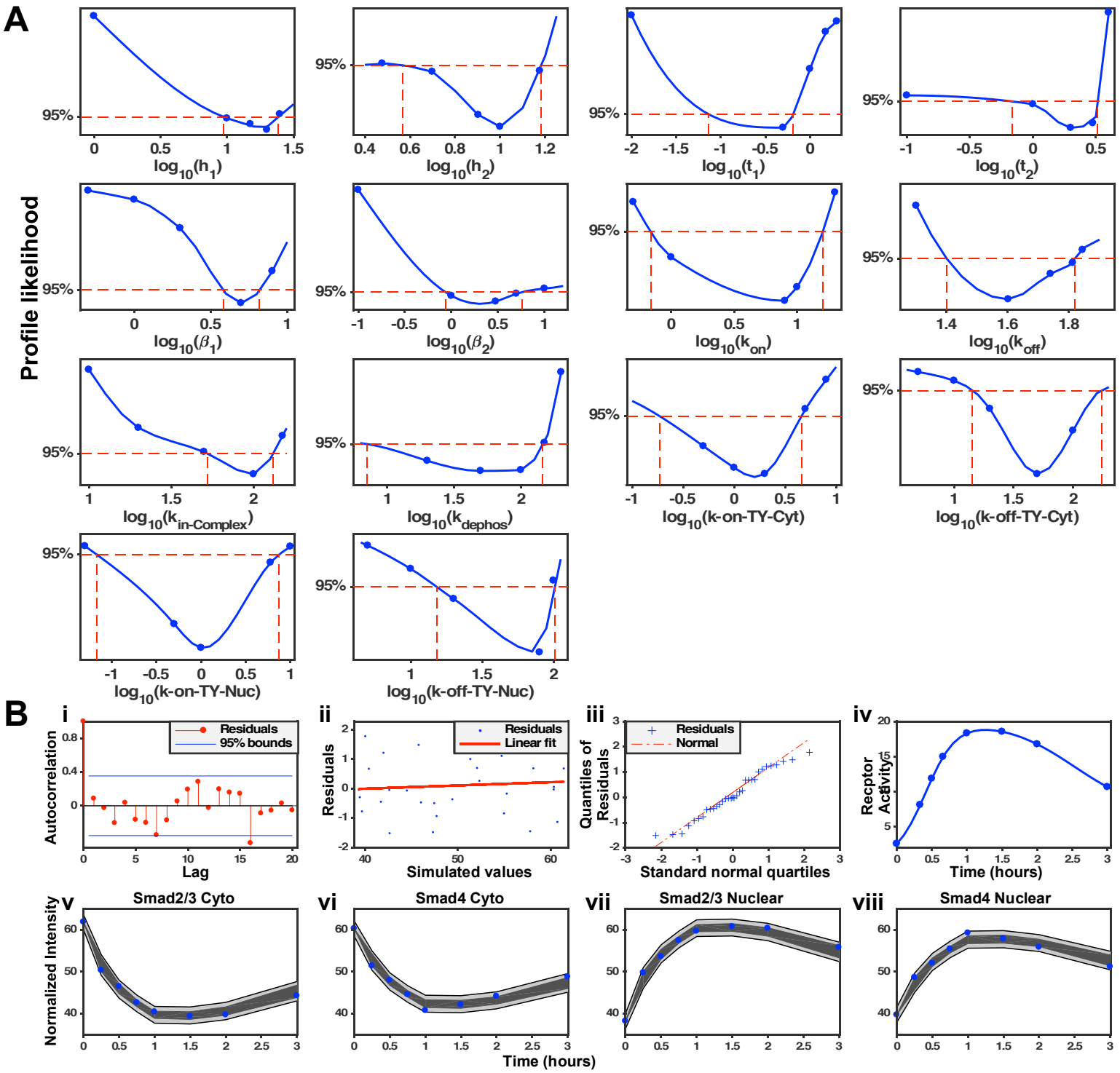

Figure S5: Profiles of the likelihood function for the model parameters and diagnostic plots for the simplified model (related to Figure 5).

(**A**) The profile likelihood for each model parameter for the simplified model was estimated by running DREAM$_{(ZS)}$ algorithm. The solid and dashed lines display profile likelihood versus parameter and 95% confidence levels, respectively. Full circles indicate the parameter vectors that have been sampled in the parameter scan. The profile likelihood of each model parameter has a unique minimum indicating parameter identifiability. **(B, i-iv)** Diagnostic plots of the residuals and the receptor activity pattern. (**i**) The residual autocorrelation function of the models are inside the 95% confidence intervals of the corresponding estimates, indicating that the residuals are uncorrelated and the whiteness test is fulfilled. (**ii**) The model residuals are plotted over the model predicted outputs. The residual plot shows no fitted pattern. (**iii**) Normal quantile-quantile plots approximately follow a straight line confirming that the residuals are normally distributed. (**iv**) The temporal pattern of the receptor activity for the best fitted parameters shows the receptor has maximum activity around 1.3 h and then declines due to negative regulation. The solid line and the full circles indicate the fitted plot and the receptor activity at sampled data, respectively. (**B, v-viii**) The 95% simulation uncertainty intervals due to parameter (dark region) and total uncertainty (light gray) and the observed values (blue circles) for cytoplasmic and nuclear Smad2/3 and Smad4 confirm that the process dynamics are captured by the model.

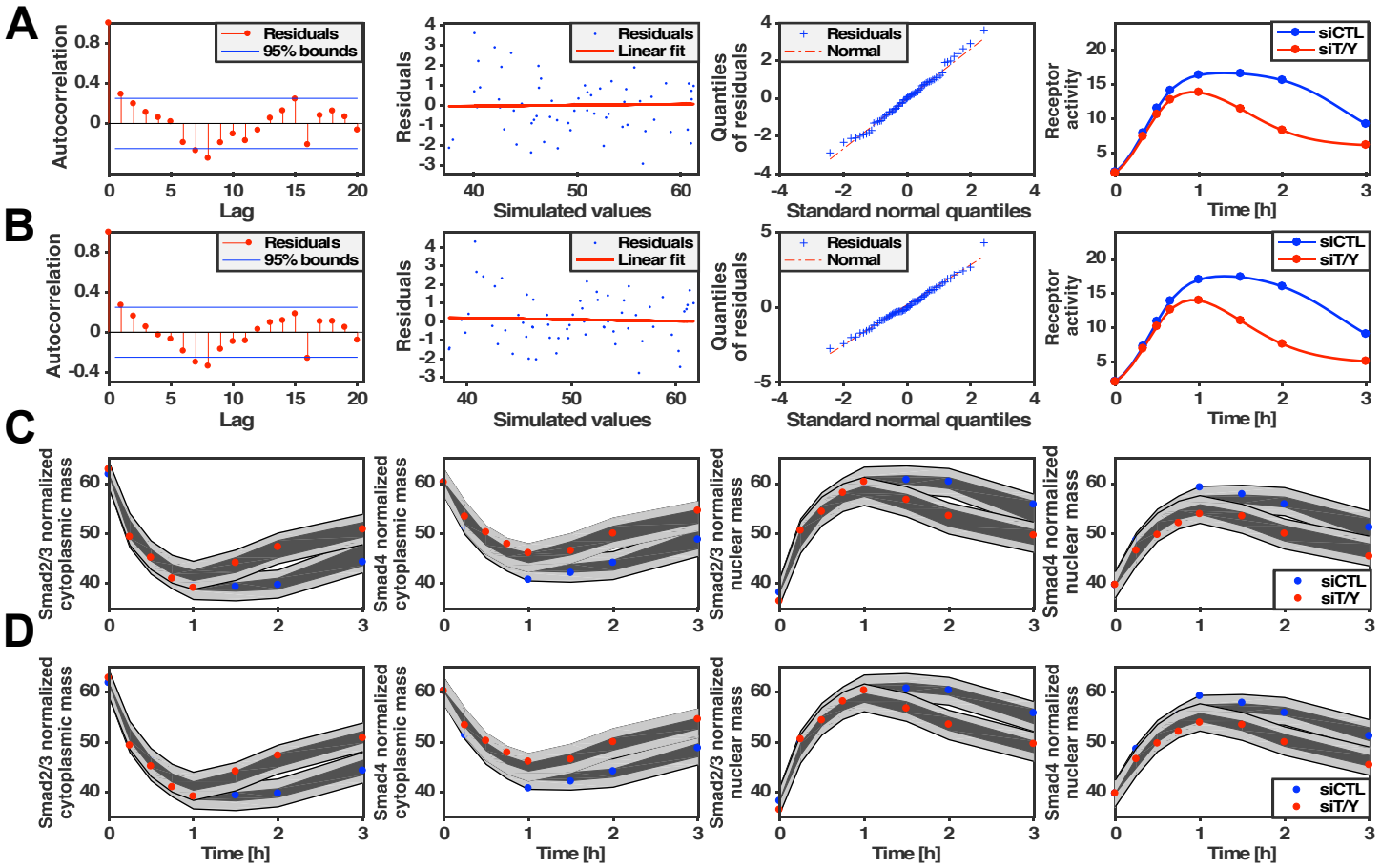

Figure S6. Diagnostic plots of the residuals, receptor activities and the 95% uncertainty ranges for the simulation data of the full and restricted RAA models (related to Figure 5).
The residual analysis for the full (**A**) and the restricted (**B**) RAA models show that the residuals of the models are uncorrelated and inside the 95% confidence intervals of the corresponding estimates, randomly distributed and show no fitted pattern. The residuals are roughly normally distributed as the normal quantile-quantile plots approximately follow a straight line. The temporal patterns of receptors of both models for both conditions initially have the same activity, however near the peak, receptor activity in cells transfected with siTaz/Yap declines faster. The solid line and the full circles indicate the fitted plot and the receptor activity at sampled data, respectively. The 95% uncertainty ranges due to parameter (dark region) and total uncertainty (light gray) and the observed values (full circles) for the simulation data of (**C**) the full and (**D**) the restricted RAA models confirm that about 95% of the observations lie within the gray region, an indication that the simulation uncertainty ranges are statistically adequate.

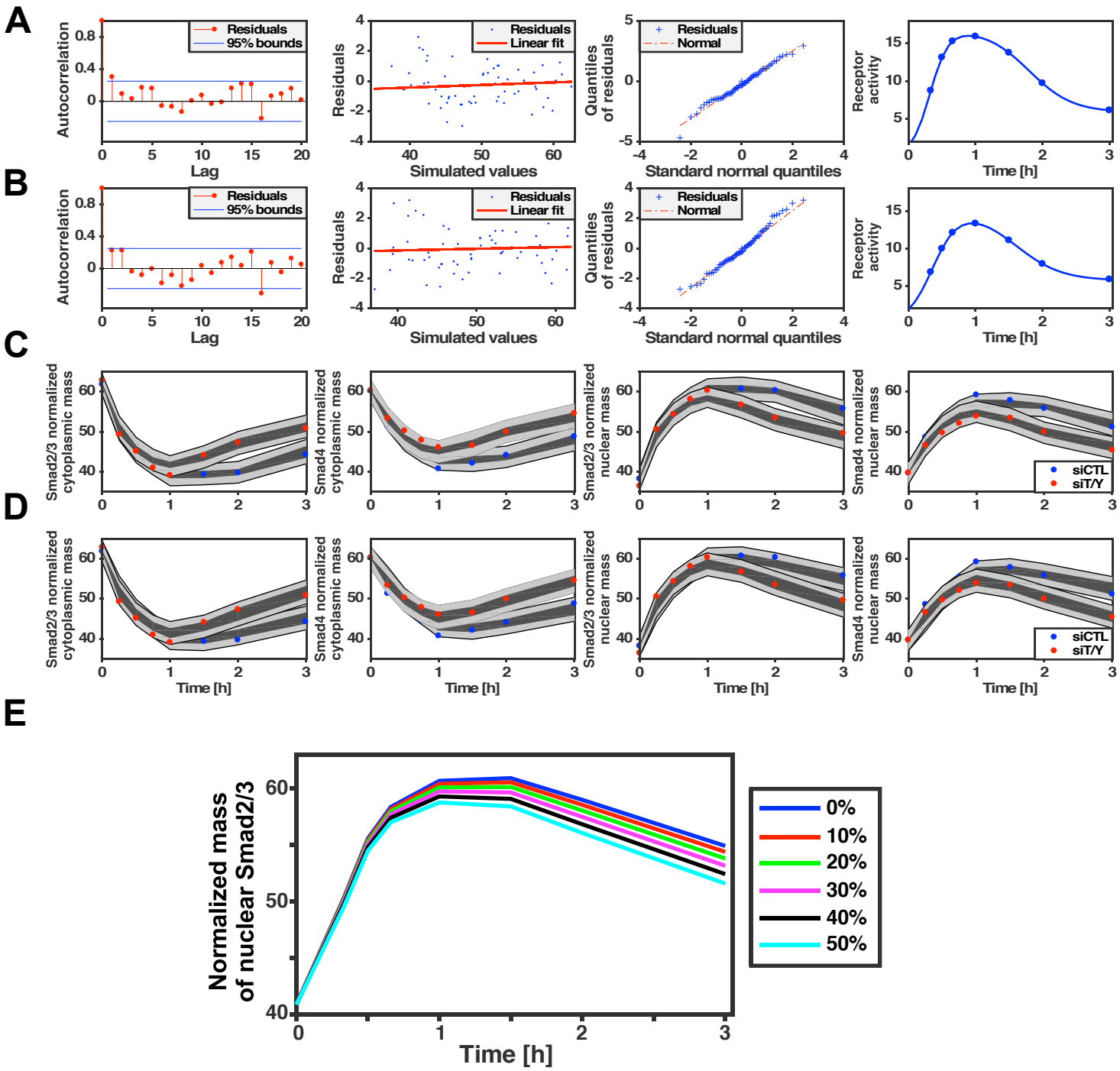

Figure S7. Residual analysis, receptor activities and the 95% uncertainty ranges for the simulation data of the CRF and DRF models and simulation of the CRF model (related to Figure 5).
The residual of the CRF (**A**) and the DRF models (**B**) are uncorrelated, random normally distributed. The receptors of two models for both conditions have the same activity. The solid line and the full circles indicate the fitted plot and the receptor activity at sampled data, respectively. The 95% uncertainty ranges for the simulation data for the CRF model (**C**) and the DRF models (**D**) confirm that the simulation uncertainty ranges are statistically adequate. The lighter and darker gray regions denote the 95% model uncertainty and the 95% parameter uncertainty bounds, respectively. The full circles denote the observed data for the model simulation data. (**E**) Simulation of the CRF model for varying concentrations of the retention factor. The concentration of the retention factor was changed from the initial value (ie no change, 0%) to 50% reduction. The simulation results are consistent with experimental observations shown in Figure 1.

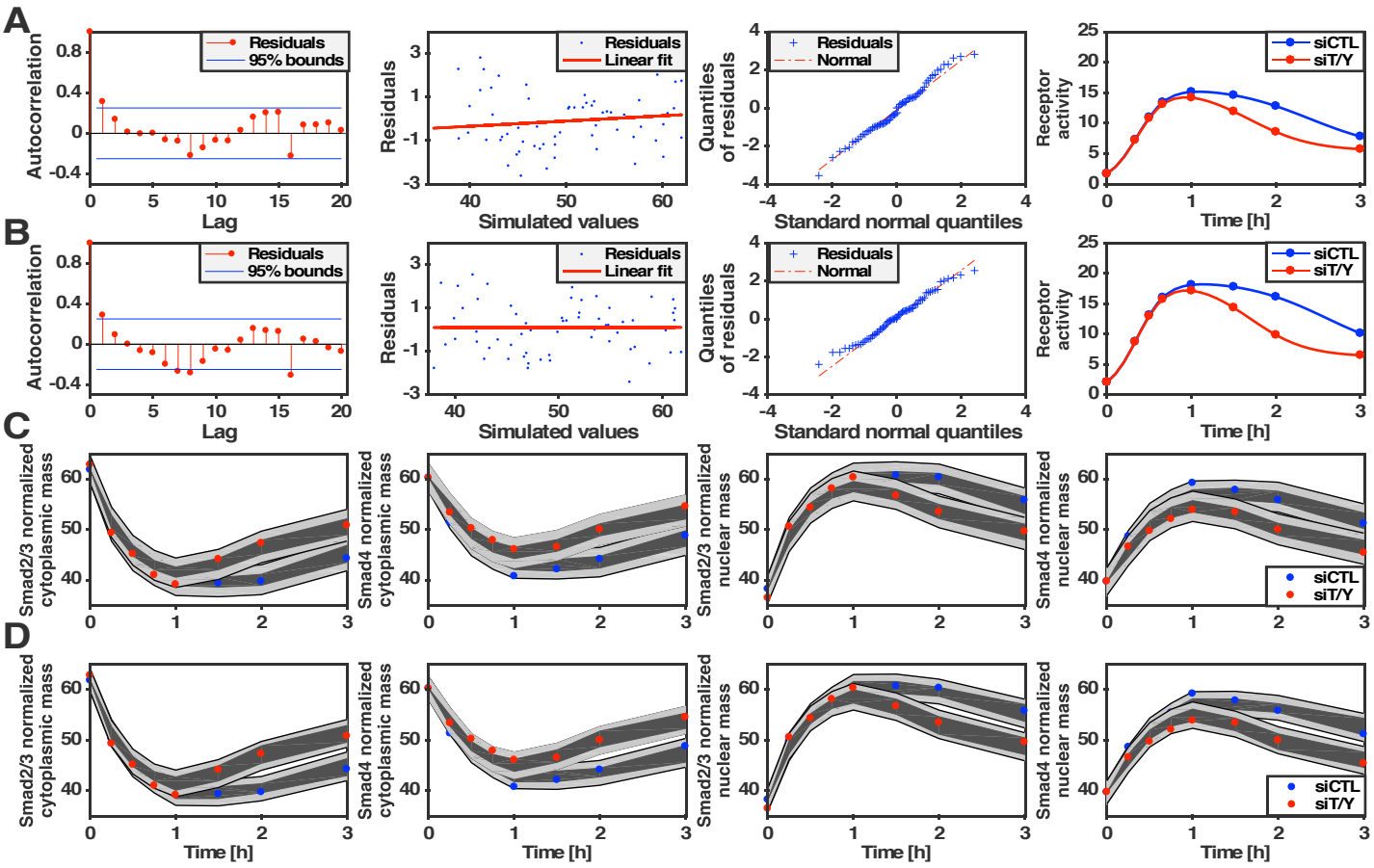

Figure S8. Residual analysis, receptor activities and the 95% uncertainty ranges for the simulation data of the RAACRF and RAADRF models (related to Figure 5).

The residual analysis for the RAACRF (**A**) and the RAADRF models (**B**) are uncorrelated, random normally distributed. The temporal patterns of receptors of two models show for cells transfected with siTaz/Yap the receptor activity declines sooner. The solid line and the full circles indicate the fitted plot and the receptor activity at sampled data, respectively. The 95% uncertainty ranges for the simulation data for the RAACRF model (**C**) and the RAADRF models (**D**) confirm that the simulation uncertainty ranges are statistically adequate. The lighter and darker gray regions denote the 95% model uncertainty and the 95% parameter uncertainty bounds, respectively. The full circles denote the observed data for the model simulation data.

Table S1: Fitting linear mixed-effects model to data of siTaz/Yap transfected cells (related to Figure 5).

Linear mixed-effects model fit by ML						
Formula: Ratio ~ 1 + Dose *Time + (1 | Id)						
Fixed effect coefficients (95% CIs):	Name	Estimate	SE	pValue	Lower	Upper
	Intercept	2.502	0.041816	3.451e-6	2.4188	2.5852
	Dose	2.7879e-05	0.001277	0.98264	-0.0025133	0.0025691
	Time	0.010914	0.018526	0.55742	-0.025953	0.047782
	Dose:Time	0.00077432	0.00082408	0.35024	-0.0024143	0.00086565
Random effects covariance parameters (95% CIs):	Name1	Name2	Type	Estimate	Lower	Upper
	Intercept	Intercept	Std	0.043	0.013315	0.13887

Table S2: Selecting the best linear regression model for data of siTaz/Yap transfected cells (related to Figure 5).

Generalized linear regression model:					
Ratio ~ 1+Id					
Estimated Coefficients	Name	Estimate	SE	tStat	pValue
	Intercept	2.3607	0.043216	54.739	2.4798e-66
	Id	0.094048	0.027276	3.4481	0.00089375

Table S3: Fitting linear mixed-effects model to data of cells seeded at 8 densities (related to Figure 5).

Linear mixed-effects model fit by ML						
Formula: Ratio ~ 1 + Dose *Time + (1 | Id)						
Fixed effect coefficients (95% CIs):	Name	Estimate	SE	pValue	Lower	Upper
	Intercept	1.8781	0.12348	7.5854e-27	1.6328	2.1233
	Dose	-0.012865	0.0157	0.41756	-0.044242	0.018512
	Time	0.00064484	0.00073734	0.38409	-0.00081957	0.0021093
	Dose:Time	0.00015873	0.00044463	0.72191	-0.00072435	0.0010418
Random effects covariance parameters (95% CIs):	Name1	Name2	Type	Estimate	Lower	Upper
	Intercept	Intercept	Std	0.3413	0.20841	0.55893

Table S4: Selecting the best linear regression model for data of cells seeded at 8 densities (related to Figure 5).

Generalized linear regression model:					
Ratio ~ 1+Id					
Estimated Coefficients	Name	Estimate	SE	tStat	pValue
	Intercept	2.5169	0.0342156	73.69	5.8628e-85
	Id	0.14055	0.00067638	-20.779	6.5425e-37

Table S5: The model parameters (related to Figure 5).

Parameter	Description
$[ARC] = (h_0 + \frac{(h_1 - h_0)}{(1 + \exp(-\beta_1(t - t_1)))})(h_2 + \frac{(h_1 - h_2)}{(1 + \exp(\beta_2(t - t_2)))})/h_1$	Activated Receptor Complex [ARC]
h_0, h_1, h_2	height parameters of the receptor
t_1 , t_2	the onset and the offset times of the receptor
β_1 , β_2	the slope parameters of the receptor
k_{on} , k_{off}	association and dissociation rates of pSmad2/3 and Smad4
$k_{in-Complex}$	nuclear import rate of the complex pSmad2/3-Smad4
k_{in}	nuclear import rate of Smad2/3, Smad4 or pSmad2/3
$k_{ex-S23} = 2.19k_{in}$	export rate of Smad2/3
$k_{ex-S4} = 2.11k_{in}$	export rate of Smad4
k_{dephos}	dephosphorylating rate
k_{in-TY}, k_{ex-TY}	import and export rates of Taz/Yap
$k_{on-TY_{Cyt}}$, $k_{off-TY_{Cyt}}$	association and dissociation rates of pSmad23-Smad4 and Taz/Yap in the cytoplasm
$k_{on-TY_{Nuc}}$, $k_{off-TY_{Nuc}}$	association and dissociation rates of pSmad23-Smad4 and Taz/Yap in the nucleus
$k_{in-pSS4TY}$	nuclear import rate of the complex pSmad23-Smad4-Taz/Yap

Table S6: Initial Model Equations (related to Figure 5).

$[ARC] = \left(h_0 + \frac{(h_1 - h_0)}{1 + \exp(-\beta_1(t - t_1))}\right)\left(h_2 + \frac{(h_1 - h_2)}{1 + \exp(\beta_2(t - t_2))}\right)/h_1$	
$R_1 = [ARC][Smad2/3_{Cyt}]$	$d[Smad2/3_{Cyt}]/dt = R_5 - R_1$
$R_2 = k_{on}[pSmad2/3_{Cyt}][Smad4_{Cyt}] - k_{off}[pSmad2/3 - Smad4_{Cyt}]$	$d[pSmad2/3_{Cyt}]/dt = R_1 - R_2 - R_8$
$R_3 = k_{in-Complex}[pSmad2/3 - Smad4_{Cyt}]$	$d[Smad4_{Cyt}]/dt = R_4 - R_2$
$R_4 = k_{ex-S4}[Smad4_{Nuc}] - k_{in}[Smad4_{Cyt}]$	$d[pSmad2/3 - Smad4_{Cyt}]/dt = R_2 - R_3 - R_{10}$
$R_5 = k_{ex-S23}[Smad2/3_{Nuc}] - k_{in}[Smad2/3_{Cyt}]$	$d[pSmad2/3 - Smad4_{Nuc}]/dt = R_3 - R_6 + R_{11}$
$R_6 = -k_{on}[pSmad2/3_{Nuc}][Smad4_{Nuc}] + k_{off}[pSmad2/3 - Smad4_{Nuc}]$	$d[Smad2/3_{Nuc}]/dt = R_7 - R_5$
$R_7 = k_{dephos}[pSmad2/3_{Nuc}]$	$d[pSmad2/3_{Nuc}]/dt = R_6 - R_7 + R_8$
$R_8 = k_{in}[pSmad2/3_{Cyt}]$	$d[Smad4_{Nuc}]/dt = R_6 - R_4$
$R_9 = k_{ex-TY}[Taz/Yap_{Nuc}] - k_{in-TY}[Taz/Yap_{Cyt}]$	$d[Taz/Yap_{Cyt}]/dt = R_9 - R_{10}$
$R_{10} = k_{on-TY-Cyt}[pSmad2/3 - Smad4_{Cyt}][Taz/Ya_{Cyt}] - k_{off-TY-Cyt}[pSmad2/3 - Smad4 - Taz/Yap_{Cyt}]$	$d[Taz/Yap_{Nuc}]/dt = R_{11} - R_9$
$R_{11} = -k_{on-TY-Nuc}[pSmad2/3 - Smad4_{Nuc}][Taz/Ya_{Nuc}] + k_{off-TY-Nuc}[pSmad2/3 - Smad4 - Taz/Yap_{Nuc}]$	$d[pSmad2/3 - Smad4 - Taz/Yap_{Cyt}]/dt = R_{10} - R_{12}$
$R_{12} = k_{in-pSS4TY}[pSmad2/3 - Smad4 - Taz/Yap_{Cyt}]$	$d[pSmad2/3 - Smad4 - Taz/Yap_{Nuc}]/dt = R_{12} - R_{11}$

Table S7: Simplified Model Equations (related to Figure 5).

$$[ARC] = \left(h_0 + \frac{(h_1 - h_0)}{1 + \exp(-\beta_1(t - t_1))}\right)\left(h_2 + \frac{(h_1 - h_2)}{1 + \exp(\beta_2(t - t_2))}\right)/h_1$$

$R_1 = [ARC][Smad2/3_{Cyt}]$	$d[Smad2/3_{Cyt}]/dt = R_5 - R_1$
$R_2 = k_{on}[pSmad2/3_{Cyt}][Smad4_{Cyt}] - k_{off}[pSmad2/3 - Smad4_{Cyt}]$	$d[pSmad2/3_{Cyt}]/dt = R_1 - R_2 - R_8$
$R_3 = k_{in-Complex}[pSmad2/3 - Smad4_{Cyt}]$	$d[Smad4_{Cyt}]/dt = R_4 - R_2$
$R_4 = k_{ex-S4}[Smad4_{Nuc}] - k_{in}[Smad4_{Cyt}]$	$d[pSmad2/3 - Smad4_{Cyt}]/dt = R_2 - R_3 - R_9$
$R_5 = k_{ex-S23}[Smad2/3_{Nuc}] - k_{in}[Smad2/3_{Cyt}]$	$d[pSmad2/3 - Smad4_{Nuc}]/dt = R_3 - R_6 + R_{10}$
$R_6 = -k_{on}[pSmad2/3_{Nuc}][Smad4_{Nuc}] + k_{off}[pSmad2/3 - Smad4_{Nuc}]$	$d[Smad2/3_{Nuc}]/dt = R_7 - R_5$
$R_7 = k_{dephos}[pSmad2/3_{Nuc}]$	$d[pSmad2/3_{Nuc}]/dt = R_6 - R_7 + R_8$
$R_8 = k_{in}[pSmad2/3_{Cyt}]$	$d[Smad4_{Nuc}]/dt = R_6 - R_4$
$R_9 = k_{on-TY-Cyt}[pSmad2/3 - Smad4_{Cyt}][Taz/Ya_{Cyt}]$ $-k_{off-TY-Cyt}[pSmad2/3 - Smad4 - Taz/Yap_{Cyt}]$	$d[pSmad2/3 - Smad4 - Taz/Yap_{Cyt}]/dt = R_9$
$R_{10} = -k_{on-TY-Nuc}[pSmad2/3 - Smad4_{Nuc}][Taz/Ya_{Nuc}]$ $+k_{off-TY-Nuc}[pSmad2/3 - Smad4 - Taz/Yap_{Nuc}]$	$d[pSmad2/3 - Smad4 - Taz/Yap_{Nuc}]/dt = -R_{10}$
$[pSmad2/3 - Smad4 - Taz/Yap_{Cyt}] + [Taz/Yap_{Cyt}] = Constant$ $[pSmad2/3 - Smad4 - Taz/Yap_{Nuc}] + [Taz/Yap_{Nuc}] = Constant$	

Table S8: RAA Model Equations (related to Figure 5).

$$[ARC] = \left(h_0 + \frac{(h_1 - h_0)}{1 + \exp(-\beta_1(t - t_1))}\right)\left(h_2 + \frac{(h_1 - h_2)}{1 + \exp(\beta_2(t - t_2))}\right)/h_1$$

$R_1 = [ARC][Smad2/3_{Cyt}]$	$d[Smad2/3_{Cyt}]/dt = R_5 - R_1$
$R_2 = k_{on}[pSmad2/3_{Cyt}][Smad4_{Cyt}] - k_{off}[pSmad2/3 - Smad4_{Cyt}]$	$d[pSmad2/3_{Cyt}]/dt = R_1 - R_2 - R_8$
$R_3 = k_{in-Complex}[pSmad2/3 - Smad4_{Cyt}]$	$d[Smad4_{Cyt}]/dt = R_4 - R_2$
$R_4 = k_{ex-S4}[Smad4_{Nuc}] - k_{in}[Smad4_{Cyt}]$	$d[pSmad2/3 - Smad4_{Cyt}]/dt = R_2 - R_3$
$R_5 = k_{ex-S23}[Smad2/3_{Nuc}] - k_{in}[Smad2/3_{Cyt}]$	$d[pSmad2/3 - Smad4_{Nuc}]/dt = R_3 - R_6$
$R_6 = -k_{on}[pSmad2/3_{Nuc}][Smad4_{Nuc}] + k_{off}[pSmad2/3 - Smad4_{Nuc}]$	$d[Smad2/3_{Nuc}]/dt = R_7 - R_5$
$R_7 = k_{dephos}[pSmad2/3_{Nuc}]$	$d[pSmad2/3_{Nuc}]/dt = R_6 - R_7 + R_8$
$R_8 = k_{in}[pSmad2/3_{Cyt}]$	$d[Smad4_{Nuc}]/dt = R_6 - R_4$

Table S9: DRF and CRF Model Equations (related to Figure 5).

$$[ARC] = \left(h_0 + \frac{(h_1 - h_0)}{1 + \exp(-\beta_1(t - t_1))}\right)\left(h_2 + \frac{(h_1 - h_2)}{1 + \exp(\beta_2(t - t_2))}\right)/h_1$$

$R_1 = [ARC][Smad2/3_{Cyt}]$	$d[Smad2/3_{Cyt}]/dt = R_5 - R_1$
$R_2 = k_{on}[pSmad2/3_{Cyt}][Smad4_{Cyt}] - k_{off}[pSmad2/3 - Smad4_{Cyt}]$	$d[pSmad2/3_{Cyt}]/dt = R_1 - R_2 - R_8$
$R_3 = k_{in-Complex}[pSmad2/3 - Smad4_{Cyt}]$	$d[Smad4_{Cyt}]/dt = R_4 - R_2$
$R_4 = k_{ex-S4}[Smad4_{Nuc}] - k_{in}[Smad4_{Cyt}]$	$d[pSmad2/3 - Smad4_{Cyt}]/dt = R_2 - R_3 - R_9$
$R_5 = k_{ex-S23}[Smad2/3_{Nuc}] - k_{in}[Smad2/3_{Cyt}]$	$d[pSmad2/3 - Smad4_{Nuc}]/dt = R_3 - R_6 + R_{10}$
$R_6 = -k_{on}[pSmad2/3_{Nuc}][Smad4_{Nuc}] + k_{off}[pSmad2/3 - Smad4_{Nuc}]$	$d[Smad2/3_{Nuc}]/dt = R_7 - R_5$
$R_7 = k_{dephos}[pSmad2/3_{Nuc}]$	$d[pSmad2/3_{Nuc}]/dt = R_6 - R_7 + R_8$
$R_8 = k_{in}[pSmad2/3_{Cyt}]$	$d[Smad4_{Nuc}]/dt = R_6 - R_4$
$R_9 = k_{on-TY-Cyt}[pSmad2/3 - Smad4_{Cyt}][Taz/Ya_{Cyt}] - k_{off-TY-Cyt}$ $[pSmad2/3 - Smad4 - Taz/Yap_{Cyt}]$	$d[pSmad2/3 - Smad4 - Taz/Yap_{Cyt}]/dt = R_9$
$R_{10} = -k_{on-TY-Nuc}[pSmad2/3 - Smad4_{Nuc}][Taz/Ya_{Nuc}] + k_{off-TY-Nuc}$ $[pSmad2/3 - Smad4 - Taz/Yap_{Nuc}]$	$d[pSmad2/3 - Smad4 - Taz/Yap_{Nuc}]/dt = -R_{10} + R_{11}$
$R_{11} = -k_{on-TY-X}[pSmad2/3 - Smad4 - Taz/Yap_{Nuc}]$ $[100 - pSmad2/3 - Smad4 - Taz/Yap - X]$ $+k_{off-TY-X}[pSmad2/3 - Smad4 - Taz/Yap - X]$	$d[Smad2/3 - Smad4 - Taz/Yap - X]/dt = -R_{11}$
$[pSmad2/3 - Smad4 - Taz/Yap_{Cyt}] + [Taz/Yap_{Cyt}] = Constant$ $[pSmad2/3 - Smad4 - Taz/Yap_{Nuc}] + [pSmad2/3 - Smad4 - Taz/Yap - X] + [Taz/Yap_{Nuc}] = Constant$	

Table S10: Statistical analysis of the ratio of import of the complexes pSmad2/3-Smad4-Taz/Yap and pSmad2/3-Smad4 and import rate of Taz/Yap (related to Figure 5).

	k_{in-TY}			$\gamma = \frac{k_{in-pSS4TY}}{k_{in-Complex}}$		
	MAP	Mean	Std	MAP	Mean	Std
siCTL	0.2672×10^{-3}	6.0596×10^{-3}	5.5411×10^{-3}	0.0454×10^{-3}	0.0200×10^{-3}	0.0167×10^{-3}
Low cell density	5.8690×10^{-3}	9.006	1.0199	0.0041×10^{-3}	7.4×10^{-3}	5.2×10^{-3}
High cell density	2.3338×10^{-3}	2.6824×10^{-3}	2.3183×10^{-3}	0.7087×10^{-3}	0.1507×10^{-3}	0.1334×10^{-3}

Table S11: Statistical analysis of the parameter set for the simplified model (related to Figure 5).

Parameter	MAP	Mean	Standard deviation
h_1	21.31	20.46	0.90
h_2	7.88	7.00	0.60
t_1	0.43	0.42	0.03
t_2	2.44	2.48	0.24
β_1	4.73	4.99	0.48
β_2	1.86	1.97	0.51
k_{on}	2.75	2.75	0.52
k_{off}	86.1	83.64	4.65
$k_{in-Complex}$	166.45	166.89	3.52
k_{dephos}	90.44	89.02	1.14
$k_{on-TY_{Cyt}}$	2.57	2.06	0.59
$k_{off-TY_{Cyt}}$	112.02	109.57	2.04
$k_{on-TY_{Nuc}}$	0.48	0.49	0.27
$k_{off-TY_{Nuc}}$	57.06	60.55	2.05
Root Mean Square Error (RMSE)	0.9213		

Table S12: The initial values of cytoplasmic and nuclear signals in the simplified model (related to Figure 5).

Signal	MAP	Mean	Standard deviation
h_0	0	0.12	0.02
[Smad2/3$_{Cyt}$]	58.11	58.43	0.84
[pSmad2/3$_{Cyt}$]	1.163	1.32	0.30
[Smad4$_{Cyt}$]	58.89	59.31	0.64
[pSmad2/3-Smad4$_{Cyt}$]	0.84	0.79	0.07
[Taz/Yap$_{Cyt}$]	49.39	49.54	0.18
[pSmad2/3-Smad4-Taz/Yap$_{Cyt}$]	0.61	0.46	0.18
[Smad2/3$_{Nuc}$]	33.88	33.35	0.41
[pSmad2/3$_{Nuc}$]	1.69	1.5040	0.12
[Smad4$_{Nu}$]	34.98	34.41	0.47
[pSmad2/3-Smad4$_{Nu}$]	3.96	3.63	0.49
[Taz/Yap$_{Nu}$]	49.51	48.84	0.59
[pSmad2/3-Smad4-Taz/Yap$_{Nu}$]	0.49	1.16	0.19

Table S13: The parameter correlation matrix of the simplified model (related to Figure 5).

	k_{on}	k_{off}	$k_{in-Complex}$	k_{dephos}	$k_{on-TY_{Cyt}}$	$k_{off-TY_{Cyt}}$	$k_{on-TY_{Nuc}}$	$k_{off-TY_{Nuc}}$
k_{on}	1	0.25	-0.01	0.02	0.30	-0.04	-0.50	0.03
k_{off}	0.25	1	-0.09	0.02	-0.05	-0.06	0.08	-0.06
$k_{in-Complex}$	-0.015	-0.09	1	0.02	0.04	-0.06	-0.09	0.02
k_{dephos}	0.02	0.02	0.02	1	-0.08	0.06	-0.04	-0.03
$k_{on-TY_{Cyt}}$	0.30	-0.05	0.04	-0.08	1	0.04	-0.02	0.005
$k_{off-TY_{Cyt}}$	-0.04	-0.06	-0.06	0.06	0.04	1	-0.01	-0.05
$k_{on-TY_{Nuc}}$	-0.50	0.08	-0.09	-0.04	-0.02	-0.01	1	-0.03
$k_{off-TY_{Nuc}}$	0.03	-0.06	0.02	-0.03	0.005	-0.05	-0.03	1

Table S14: Statistical analysis of the parameter sets for the RAA models (related to Fig 5).

	Full model			Restricted model		
Parameter	Maximum a posteriori	Mean	Standard deviation	Maximum a posteriori	Mean	Standard deviation
h_1	sC: 17.04, sTY:16.08	sC: 17.41, sTY:16.85	sC: 1.09, sTY:1.18	21.93	19.80	1.99
h_2	sC: 5.57, sTY: 5.98	sC: 5.52, sTY:5.89	sC: 0.30, sTY:0.52	5.70	5.66	0.50
t_1	sC: 0.36, sTY:0.36	sC: 0.36, sTY: 0.35	sC: 0.03, sTY: 0.03	0.42	0.40	0.03
t_2	sC: 2.72, sTY: 1.56	sC:2.73, sTY:1.49	sC: 0.17, sTY:0.10	sC:2.69, sTY:1.45	sC: 2.69, sTY:1.45	sC: 0.15, sTY:0.12
β_1	sC: 5.30, sTY:5.31	sC: 5.26,sTY:5.49	sC: 0.6 sTY:0.28	4.89	5.29	0.37
β_2	sC:2.72, sTY:2.75	sC:2.80, sTY:2.49	sC:0.58, sTY:0.29	2.38	2.18	0.36
k_{on}	6.15	6.80	0.55	5.84	6.35	1.00
k_{off}	66.05	65.80	2.88	68.16	66.08	4.04
$k_{in-Complex}$	50.11	48.99	1.21	44.62	45.30	1.91
k_{dephos}	117.21	116.26	1.79	108.00	107.56	2.65
Root Mean Square Error (RMSE)	1.3539			1.3419		

Table S15: Initial values of cytoplasmic and nuclear signals in the RAA models (related to Figure 5).

	Full model						Restricted model					
Complex	Maximum a posterior (MAP)		Mean		Standard deviation		Maximum a posterior (MAP)		Mean		Standard deviation	
	sC	sTY	sC	sTY	sC	sTY	sC	sTY	sC	sTY	sC	sTY
h_0	0	0	0	0	0	0	0	0	0	0	0	0
$[Smad2/3_{Cyt}]$	57.3	57.7	57.43	57.58	1.29	1.12	56.89	57.22	57.10	57.42	1.07	1.26
$[Smad4_{Cyt}]$	58.43	58.70	58.59	58.71	0.85	0.77	58.16	58.39	58.43	58.66	0.78	0.95
$[pSmad2/3_{Cyt}]$	0.72	0.69	0.66	0.12	0.13	0.82	0.82	0.79	0.76	0.74	0.19	0.18
$[pSmad2/-Smad4_{Cyt}]$	2.51	2.42	2.48	0.21	0.23	2.81	2.81	2.72	2.62	2.54	0.26	0.25
$[Smad2/3_{Nuc}]$	33.87	33.82	33.66	0.68	0.54	33.78	33.78	33.74	33.51	33.47	0.54	0.67
$[Smad4_{Nuc}]$	32.52	32.43	32.37	0.44	0.43	32.38	32.38	32.46	32.18	32.25	0.48	0.46
$[pSmad2/3_{Nuc}]$	1.12	1.07	1.08	0.097	0.07	1.22	1.22	1.19	1.20	1.17	0.13	0.13
$[pSmad2/-Smad4_{Nuc}]$	5.61	5.4	5.69	5.61	0.48	0.47	5.63	5.45	5.90	5.72	5.58	0.55

Table S16: The parameter correlation matrix for the RAA full model (related to Figure 5).

	k_{on}	k_{off}	$k_{in-Complex}$	k_{dephos}
k_{on}	1	0.28	-0.13	0.11
k_{off}	0.28	1	-0.03	-0.02
$k_{in-Complex}$	-0.13	-0.03	1	-0.01
k_{dephos}	0.12	-0.02	-0.01	1

Table S17: The parameter correlation matrix for the RAA restricted model (related to Figure 5).

	k_{on}	k_{off}	$k_{in-Complex}$	k_{dephos}
k_{on}	1	0.51	-0.32	-0.13
k_{off}	0.51	1	-0.25	-0.16
$k_{in-Complex}$	-0.32	-0.25	1	0.31
k_{dephos}	-0.13	-0.16	0.31	1

Table S18: Statistical analysis of the parameter sets for the CRF and DRF models (related to Figure 5).

	CRF model			DRF model		
Parameter	Maximum a posteriori	Mean	Standard deviation	Maximum a posteriori	Mean	Standard deviation
h_1	16.89	17.37	1.98	15.20	21.84	5.01
h_2	5.88	6.10	0.85	5.73	4.63	0.98
t_1	0.32	0.34	0.03	0.37	0.39	0.05
t_2	1.80	1.724	0.14	1.59	1.54	0.31
β_1	7.32	7.00	0.52	5.33	5.41	0.45
β_2	3.09	3.06	0.57	2.92	1.73	0.53
k_{on}	2.73	3.14	0.91	6.88	3.94	1.3716
k_{off}	88.92	96.63	8.21	99.28	87.97	9.16
$k_{in-Complex}$	151.36	136.40	11.04	120.30	134.02	9.06
k_{dephos}	110.43	95.95	8.25	117.77	124.63	11.49
$k_{on-TY_{Cyt}}$	2.55	1.74	0.71	0.36	0.68	0.38
$k_{off-TY_{Cyt}}$	22.43	19.62	9.11	10.76	11.33	2.81
$k_{on-TY_{Nuc}}$	0.16	0.17	0.09	0.07	0.11	0.078
$k_{off-TY_{Nuc}}$	93.09	108.92	10.82	46.89	33.09	8.93
$k_{on-TY-X}$	19.57	18.82	2.12	1.19	1.27	0.521
$k_{off-TY-X}$	16.19	12.36	2.90	2.53	2.99	1.10
α	-	-	-	0.38	0.54	0.12
Root Mean Square Error (RMSE)	1.4138			1.3933		

Table S19: The initial values of cytoplasmic and nuclear signals in the CRF and DRF models (related to Figure 5).

	CRF model						DRF model					
Complex	Maximum a posterior (MAP)		Mean		Standard deviation		Maximum a posterior (MAP)		Mean		Standard deviation	
	sC	sTY	sC	sTY	sC	sTY	sC	sTY	sC	sTY	sC	sTY
h_0	0	0	0	0	0	0	0	0	0	0.66	0	0
$[Smad2/3_{Cyt}]$	55.34	60.24	55.42	58.87	0.82	1.32	55.82	58.22	56.18	58.90	1.03	0.39
$[Smad4_{Cyt}]$	56.79	61.10	56.80	58.73	0.69	1.31	58.03	60.02	58.1	60.48	0.85	0.96
$[pSmad2/3_{Cyt}]$	0.91	0.91	0.79	1.04	0.11	0.35	1.50	1.44	1.37	1.44	0.19	0.28
$[pSmad2 /-Smad4_{Cyt}]$	0.52	0.54	0.78	1.37	0.07	0.82	1.18	1.21	0.94	1.01	0.11	0.18
$[Taz/Yap_{Cyt}]$	47.59	4.76	47.38	4.57	0.38	0.24	48.80	4.89	48.6	4.83	0.46	0.06
$[pSmad2/3-Smad4 -Taz/Yap_{Cyt}]$	3.15	0.29	2.61	0.43	0.38	0.24	1.19	0.11	1.40	0.16	0.46	0.06
$[Smad2/3_{Nuc}]$	29.98	32.51	30.91	32.73	0.57	1.08	33.49	34.96	32.87	34.49	0.4	0.27
$[Smad4_{Nuc}]$	28.74	31.02	29.77	31.85	0.55	1.84	32.29	33.51	31.63	35.35	0.34	1.75
$[pSmad2/3_{Nuc}]$	0.67	0.74	1.04	1.20	0.13	0.32	1.11	1.16	0.93	0.91	0.05	0.12
$[pSmad2/3 -Smad4_{Nuc}]$	1.14	1.32	2.38	3.17	0.51	0.76	2.89	3.10	2.26	2.48	0.59	0.54
$[Taz/Yap_{Nuc}]$	42.84	4.76	42.94	3.42	1.21	0.77	46.23	4.2	44.91	4.21	0.64	0.65
$[pSmad2/3-Smad4 -Taz/Yap_{Nuc}]$	0.09	0.04	0.05	0.01	0.02	0.01	0.46	0.02	0.13	0.03	0.053	0.02
$[pSmad2/-Sma -Taz/Yap-X]$	9.02	3.84	7.00	1.57	1.19	0.76	3.72	0.78	4.96	0.76	0.60	0.63
$[X]$	92.89	99.76	93.00	98.43	1.19	0.76	96.28	38.58	95.04	53.51	0.60	5.60

Table S20: The parameter correlation matrix for the CRF model (related to Figure 5).

	k_{on}	k_{off}	$k_{in-Complex}$	k_{dephos}	$k_{on-TY_{Cyt}}$	$k_{off-TY_{Cyt}}$	$k_{on-TY_{Nuc}}$	$k_{off-TY_{Nuc}}$	$k_{on-TY-X}$	$k_{off-TY-X}$
k_{on}	1	0.53	-.045	-0.03	-0.37	-0.03	-0.46	0.09	-0.11	-0.57
k_{off}	0.53	1	-0.11	0.15	-0.36	-0.34	0.08	0.18	-0.24	-0.32
$k_{in-Complex}$	-0.45	-0.11	1	0.30	0.14	-0.06	0.27	-0.07	-0.03	0.20
k_{dephos}	-0.03	0.15	0.30	1	-0.27	-0.27	0.12	0.25	0.02	0
$k_{on-TY_{Cyt}}$	-0.37	-0.36	0.14	-0.27	1	0.45	0.41	-0.14	-0.05	0.31
$k_{off-TY_{Cyt}}$	-0.03	-0.34	-0.06	-0.27	0.45	1	-0.47	-0.22	0.07	0.10
$k_{on-TY_{Nuc}}$	-0.46	0.08	0.27	0.12	0.41	-0.47	1	0.01	-0.2	0.35
$k_{off-TY_{Nuc}}$	0.09	0.18	-0.07	0.25	-0.14	-0.22	0.01	1	0.19	-0.31
$k_{on-TY-X}$	-0.11	-0.24	-0.03	0.02	-0.05	0.07	-0.2	0.19	1	0.32
$k_{off-TY-X}$	-0.57	-0.32	0.20	0	0.31	0.10	0.35	-0.31	0.32	1

Table S21: The parameter correlation matrix for the DRF model (related to Figure 5).

	k_{on}	k_{off}	$k_{in-Complex}$	k_{dephos}	$k_{on-TY_{Cyt}}$	$k_{off-TY_{Cyt}}$	$k_{on-TY_{Nuc}}$	$k_{off-TY_{Nuc}}$	$k_{on-TY-X}$	$k_{off-TY-X}$	α
k_{on}	1	0.32	0	-0.13	-0.05	0.16	-0.30	0.04	0.1	-0.09	0
k_{off}	0.32	1	-0.08	-0.11	-0.23	0.07	-0.13	0.02	-0.09	-0.17	-0.07
$k_{in-Complex}$	0	-0.08	1	0.14	-0.21	-0.28	-0.40	-0.13	0.27	-0.06	-0.21
k_{dephos}	-0.13	-0.11	0.14	1	-0.16	-0.12	-0.12	0.04	0.01	0.064	-0.21
$k_{on-TY_{Cyt}}$	-0.05	-0.23	-0.21	-0.16	1	0.59	0.45	-0.43	-0.17	0.22	0.22
$k_{off-TY_{Cyt}}$	0.16	0.07	-0.28	-0.12	0.59	1	0.22	-0.37	-0.22	0.02	0.34
$k_{on-TY_{Nuc}}$	-0.3	-0.13	-0.4	-0.12	0.45	0.22	1	-0.07	-0.57	0.09	-0.01
$k_{off-TY_{Nuc}}$	0.04	0.02	-0.13	0.04	-0.43	-0.37	-0.07	1	0.2	-0.22	-0.23
$k_{on-TY-X}$	0.1	-0.09	0.27	0.01	-0.17	-0.22	-0.57	0.20	1	0.50	-0.21
$k_{off-TY-X}$	-0.09	-0.17	-0.06	0.06	0.22	0.02	0.09	-0.22	0.50	1	-0.16
α	0	-0.07	-0.21	-0.23	0.22	0.34	-0.01	-0.23	-0.21	-0.16	1

Table S22: Statistical analysis of the parameter sets for the RAACRF and RAADRF models (related to Figure 5).

	RAACRF model			RAADRF model		
Parameter	Maximum a posteriori	Mean	Standard deviation	Maximum a posteriori	Mean	Standard deviation
h_1	16.06	15.79	2.09	19.00	18.43	1.93
h_2	5.43	5.51	1.01	6.27	5.55	0.81
t_1	0.36	0.35	0.03	0.36	0.37	0.03
t_2	sC: 2.40, sTY: 1.67	sC: 2.66, sTY: 1.61	sC: 0.21, sTY: 0.22	sC: 2.66, sTY: 1.69	sC:2.53, sTY:1.60	sC: 0.22, sTY: 0.18
β_1	5.87	5.76	0.59	5.85	6.00	0.48
β_2	sC: 2.06, sTY: 2.65	sC: 3.14, sTY: 2.68	sC: 0.7175, sTY: 0.7857	sC: 2.07, sTY: 3.00	sC: 2.25, sTY:2.42	sC: 0.49, sTY:0.68
k_{on}	4.12	4.71	1.32	4.41	4.06	1.34
k_{off}	69.19	63.66	4.21	53.35	64.17	5.61
$k_{in-Complex}$	79.15	70.37	4.82	86.17	80.11	3.70
k_{dephos}	96.97	95.86	4.82	133.77	124.604	3.53
$k_{on-TY_{Cyt}}$	1.36	1.13	0.59	0.27	1.08	0.52
$k_{off-TY_{Cyt}}$	43.71	45.38	2.64	46.77	47.94	5.55
$k_{on-TY_{Nuc}}$	0.59	0.43	0.43	0.05	0.16	0.16
$k_{off-TY_{Nuc}}$	182.35	176.67	8.92	86.61	90.85	2.75
$k_{on-TY-X}$	5.75	6.59	1.04	5.36	4.20	1.28
$k_{off-TY-X}$	52.21	54.64	4.70	23.33	21.23	3.05
α	-	-	-	0.69	0.76	0.065
Root Mean Square Error (RMSE)	1.3836			1.573		

Table S23: The initial values of cytoplasmic and nuclear signals in the RAACRF and RAADRF models (related to Figure 5).

	RAACRF model						RAADRF model					
Complex	Maximum a posterior (MAP)		Mean		Standard deviation		Maximum a posterior (MAP)		Mean		Standard deviation	
	sC	sTY	sC	sTY	sC	sTY	sC	sTY	sC	sTY	sC	sTY
h_0	0	0	0	0	0	0	0	0	0	0	0	0
$[Smad2/3_{Cyt}]$	56.15	58.92	55.45	58.87	0.1.40	10.79	55.99	57.77	56.64	58.33	0.85	1.07
$[Smad4_{Cyt}]$	57.36	59.57	56.64	59.69	1.18	1.15	57.81	59.29	57.90	59.48	0.68	1.61
$[pSmad2/3_{Cyt}]$	0.75	0.74	0.65	0.66	0.15	0.17	1.25	1.1.26	0.86	0.96	0.19	0.29
$[pSmad2 /-Smad4_{Cyt}]$	1.39	1.44	1.41	1.48	0.32	0.34	1.76	1.81	1.58	1.84	0.35	0.64
$[Taz/Yap_{Cyt}]$	48.07	4.80	47.70	4.72	0.83	0.21	48.96	4.89	48.57	4.81	0.39	0.12
$[pSmad2/3 - Smad4 - Taz/Yap_{Cyt}]$	1.93	0.20	2.30	0.28	0.83	0.22	1.04	0.11	1.43	0.19	0.39	0.12
$[Smad2/3_{Nuc}]$	32.18	33.71	31.33	32.99	0.85	0.54	34.30	35.34	33.01	33.79	0.62	0.80
$[Smad4_{Nuc}]$	30.94	32.14	30.17	32.75	0.79	1.14	33.00	33.87	31.75	33.53	0.61	0.95
$[pSmad2/3_{Nuc}]$	1.12	1.16	1.15	1.19	0.16	0.14	1.09	1.12	1.13	1.16	0.14	0.15
$[pSmad2/3 - Smad4_{Nuc}]$	3.91	4.16	4.23	4.64	1.03	0.77	3.42	3.57	3.84	4.15	0.65	0.60
$[Taz/Yap_{Nuc}]$	46.25	4.758	45.37	4.49	2.12	0.29	47.69	4.83	47.37	4.82	1.12	0.12
$[pSmad2/3 - Smad4 - Taz/Yap_{Nuc}]$	0.34	0.04	0.54	0.06	0.08	0.04	0.09	0	0.49	0.05	0.06	0.024
$[pSmad2/-Smad - Taz/Yap - X]$	3.40	0.39	4.09	0.45	1.74	0.24	2.21	0.16	2.13	0.12	0.76	0.08
$[X]$	96.60	99.61	95.91	99.55	1.74	0.24	97.78	73.28	97.87	58.13	0.76	0.08

Table S24: The parameter correlation matrix for the RAACRF model (related to Figure 5).

	k_{on}	k_{off}	$k_{in-Complex}$	k_{dephos}	$k_{on-TY_{Cyt}}$	$k_{off-TY_{Cyt}}$	$k_{on-TY_{Nuc}}$	$k_{off-TY_{Nuc}}$	$k_{on-TY-X}$	$k_{off-TY-X}$
k_{on}	1	0.27	-.040	-0.41	-0.15	-0.16	-0.49	0.22	0.28	-0.14
k_{off}	0.27	1	0.01	-0.19	0.16	0.10	0.09	0.05	0.22	-0.05
$k_{in-Complex}$	-0.40	0.01	1	-0.08	-0.09	0.16	-0.15	-0.36	0.22	-0.17
k_{dephos}	-0.41	-0.19	-0.08	1	0.32	0.05	0.51	0.02	-0.55	0.08
$k_{on-TY_{Cyt}}$	-0.15	0.16	-0.09	0.32	1	-0.15	0.75	0.22	-0.42	0.04
$k_{off-TY_{Cyt}}$	-0.16	0.10	0.16	0.05	-0.15	1	-0.14	-0.26	0.28	-0.10
$k_{on-TY_{Nuc}}$	-0.49	0.09	-0.15	0.51	0.75	-0.14	1	0.09	-0.61	0.30
$k_{off-TY_{Nuc}}$	0.22	0.05	-0.36	0.02	0.22	-0.26	0.09	1	0	-0.09
$k_{on-TY-X}$	0.28	0.22	0.22	-0.55	-0.42	0.28	-0.61	0	1	-0.27
$k_{off-TY-X}$	-0.14	-0.05	-0.17	0.08	0.04	-0.1	0.30	-0.09	-0.27	1

Table S25: The parameter correlation matrix for the RAADRF model (related to Figure 5).

	k_{on}	k_{off}	$k_{in-Complex}$	k_{dephos}	$k_{on-TY_{Cyt}}$	$k_{off-TY_{Cyt}}$	$k_{on-TY_{Nuc}}$	$k_{off-TY_{Nuc}}$	$k_{on-TY-X}$	$k_{off-TY-X}$	α
k_{on}	1	0.65	-0.36	-0.39	0.54	0.22	-0.28	0.49	-0.12	-0.34	-0.08
k_{off}	0.65	1	-0.27	-0.41	0.42	0.50	-0.15	0.25	0	-0.45	0.05
$k_{in-Complex}$	-0.36	-0.27	1	0.62	-0.10	-0.48	0.25	-0.32	-0.37	0.23	-0.47
k_{dephos}	-0.39	-0.41	0.62	1	0.04	-0.40	0.35	-0.27	-0.14	0.22	-0.10
$k_{on-TY_{Cyt}}$	0.54	0.42	-0.10	0.04	1	0	0.49	0.39	-0.27	0	-0.01
$k_{off-TY_{Cyt}}$	0.22	0.50	-0.48	-0.40	0	1	-0.46	0.20	0.48	-0.38	0.34
$k_{on-TY_{Nuc}}$	-0.28	-0.15	0.25	0.35	0.49	-0.46	1	-0.18	-0.41	0.42	0
$k_{off-TY_{Nuc}}$	0.49	0.25	-0.32	-0.27	0.39	0.20	-0.18	1	-0.09	-0.20	0.1
$k_{on-TY-X}$	-0.12	0	-0.37	-0.14	-0.27	0.48	-0.41	-0.09	1	-0.23	0.25
$k_{off-TY-X}$	-0.34	-0.45	0.23	0.22	0	-0.38	0.42	-0.20	-0.23	1	0.1
α	-0.08	0.05	-0.47	-0.10	-0.01	0.34	0	0.1	0.25	0.1	1

Table S26: The estimated weights of the three proposed models (related to Figure 5).

	RAA model (restricted model)	CRF model	RAADRF model
Weight	0.005+/-0.124	0.227+/-0.130	0.766+/-0.163

TRANSPARENT METHODS

Cell culture and transfections.

For cell culturing, EpH4 cells were grown in DMEM supplemented with 10% FBS. Cells were starved with 0.1% serum containing media for 3 h and then treated with different doses of TGFβ for varying times. Cells were transfected with Dharmacon siGENOME pools of four individual siRNAs (Thermo Scientific), against Taz (Wwtr1) (MU-041057-01) and Yap1 (MU-046247-01) (siTaz/Yap) or siControl (siCTL) in a 20 μM stock solution using Lipofectamine RNAiMAX (Life Technologies) and Opti-MEM (Life Technologies) according to the manufacturer's instructions. To ensure the same confluency for cells transfected with siCTL or siTaz/Yap and to avoid Hippo pathway activation due to high cell density, cells transfected with siCTL or siTaz/Yap were seeded at a 1:1.2 ratio (ie 25000 and 30000 cells/cm^2, respectively, per well in 6-well plates or 20,000 and 24,000 cell/cm^2, respectively, in 96-well plates). After 20 h the media was changed. After 4 h, cells were starved with 0.1% serum-containing media for 3 h and then were treated with different doses of TGFβ at different time points as indicated.

Immunoblotting.

Cells were lysed in lysis buffer (50 mM Tris–HCl, 150 mM NaCl, 1 mM EDTA, 0.5% Triton X-100, 1 mM DTT containing phosphatase and protease inhibitors). Lysates were separated on SDS-PAGE gels, and immunoblotting was performed using standard protocols as previously described (Labbe, Letamendia et al. 2000). The antibodies used were as follows: rabbit anti-Smad2/3 (Cell Signaling Technology (CST) mAb #8685); rabbit anti-phospho-Smad2/3 (Cell Signaling Technology (CST) mAb #8828); mouse anti-Smad4 (Santa Cruz #sc-7966), mouse anti-YAP (Santa Cruz #sc-101199) and anti-phospho-YAP (Ser127) (Cell Signaling Technology (CST)

#13008), rabbit anti-HSP90 (Cell Signaling Technology (CST) mAb #4874) and mouse anti-BAF170 (Santa Cruz #sc-17838). For subcellular fractionation, cells were scraped prior to lysis using NE-PER Nuclear and Cytoplasmic Reagents (ThermoFisher Scientific #78833). Protein levels, relative to control proteins, were quantitated using ImageJ.

Quantitative real-time PCR.

Total RNA was purified using PureLink RNA Mini Kit (Life Technologies), and cDNA was synthesized using 1 μg of purified RNA using Oligo-dT primers and M-MLV Reverse Transcriptase (Invitrogen #28025-013). Real-time PCR was performed using the SYBR Green master mix (Applied Biosystems) on the ABI QuantStudio 6 Flex Real-Time PCR System (Applied Biosystems). Relative gene expression was quantified by ΔΔCt method and normalized to Hprt. The sequences of the primers used are listed in the table below.

Sequence of qRT-PCR primers used in this study.

Gene	Primer Name	Primer Sequence
Ankrd1	Forward:	TGCGATGAGTATAAACGGACG
	Reverse:	GTGGATTCAAGCATATCTCGGAA
Cyr61	Forward:	CTGCGCTAAACAACTCAACGA
	Reverse:	GCAGATCCCTTTCAGAGCGG
Hprt	Forward:	TCAGTCAACGGGGGACATAAA
	Reverse:	GGGGCTGTACTGCTTAACCAG
Med18	Forward:	ACCATTAACATGATGGAGTACC
	Reverse:	GTGATCAAGGAAGGTCTCAG
Taz	Forward:	GTATCCCAGCCAAATCTCGTGATG
	Reverse:	CAGCGCATTGGGCATACTCATG
TgfβrI	Forward:	CCCTGAAGTTCTAGATGATTCC
	Reverse:	TTCAACCGATGGATCAGAAG
TgfβrII	Forward:	GTGGGAGAAGTGAAGGATTAC
	Reverse:	CAAAGTCTCACACACGATCT
Yap	Forward:	CCCTTTCTTAACAGTGGCACC
	Reverse:	GTTGAGGAAGTCGTCTGGGG
Med12l	PrimePCRTM SYBR ® Green Assay: Med12l, Mouse, BioRad, #10025636	

High-content imaging and analysis

For automated IF imaging to track subcellular localization of proteins, cells were seeded in high optical quality μ-Plate 96 well dishes (Ibidi #89626). After starvation and treatment with TGFβ for varying time points, cells were fixed with 4% paraformaldehyde, permeabilized with 0.5% Triton X-100 in PBS, and blocked in 2% BSA-PBS prior to addition of antibodies and co-staining with DAPI. Antibodies used include rabbit anti-Smad2/3 (Cell Signaling Technology (CST) mAb #8685), 1:500; mouse anti-Smad4 (Santa Cruz #sc-7966), 1:250 and mouse anti-YAP (Santa Cruz #sc-101199), 1:300. Antibody specificity and low background signals (roughly 5% of total intensity) were confirmed by testing all individual primary and secondary antibodies. Optimal activation of TGFβ signaling occurs in low serum conditions, possibly due to the presence of latent TGFβ in Fetal bovine serum (FBS) (Oida and Weiner 2010). However, the Hippo pathway can be activated in response to prolonged serum deprivation. Thus, for all studies cells in each well were starved for 3 h prior to TGFβ treatment. Images were collected using IN Cell Analyzer 6000 (GE Healthcare), equipped with a Nikon 60X/0.70 NA Plan Fluor or 20x / 0.75 NA objective and a sCMOS 2048x2048 camera. Image analysis was performed using custom image analysis routine for Columbus Image Data Storage and Analysis System v2.3 (PerkinElmer). Briefly, median fluorescence intensities of Smads and/or Taz/Yap within the nucleus and cytoplasm were calculated and then, the ratio of nuclear to cytoplasmic intensities in each individual cell was determined. Decreased Taz/Yap signal was routinely observed in about 90% of cells. Finally, the median of these ratios, in at least 1000 cells/well was calculated.

Linear mixed-effects and regression model modelling of Taz/Yap localization.

Linear mixed-effects modelling (Pinero and Bates 2000, Gelman and Hill 2006) (fitlme) as provided in Matlab (www.Mathworks.com) was used to determine effects of time, dose and

conditions that influence Taz/Yap nuclear to cytoplasmic ratio. For this, representative experiments of EpH4 cells transfected with siCTL or siTaz/Yap and treated with 1 to 50 pM TGFβ for 0 to 3 h (as in Figure 1) or cells plated at increasing densities and treated with 5 and 50 pM TGFβ (as in Figure S2) was subjected to analysis. The time and dose factors were selected as fixed effects and conditions (Id (siCTL versus siTaz/Yap)) as random, the latter of which act like additional error terms (see Table S1 and S3). In addition, stepwise regression modeling (Hox, Moerbeek et al. 2017) (the Matlab command stepwiseglm), was used to determine which variables to include in the model, and yielded a Ratio ~ 1 + Id, where Id is the condition label, as the best model (see Tables S2 and S4).

Mathematical modelling of Smad nuclear accumulation.

Smads and Taz/Yap are abundant, thus, we selected a model using deterministic ordinary differential equations (ODE) based on the conservation of mass (Edelstein-Keshet 2005). The proposed model includes the binding of Taz/Yap to the complex of pSmad2/3-Smad4, which forms upon activation of the pathway by TGFβ addition (Figure 5). Consistent with experimental findings, in the model, ligand binding to the cell-surface TgfβrII receptor allows the constitutively active TgfβrII to associate with and then phosphorylate the intracellular kinase domain of TgfβrI, which then propagates the signal by phosphorylating the downstream signal transducers, Smad2/3 proteins. Due to the presence of low levels of endogenous TGFβ, the receptor complex has some basal activity. TGFβ signaling can be regulated at multiple levels including activation and destruction of functional TGFβ receptor complexes as well as post-translational mechanisms that provide negative regulation to the receptors that terminates signaling (Moustakas and Heldin 2009). Hence, TGFβ receptor activity has onset and offset responses during TGFβ stimulation. To model the activated receptor, we used the impulse model, a 7-parameter double-sigmoid function

designed to encode precisely this type of behavior as a product of two sigmoid functions, one that captures the onset response, and another that models the offset one (Figure S4A) (Chechik and Koller 2009). The selected model for modelling TGFβ and Hippo pathway crosstalk is a general one initially selected and then refined based on new findings. In the model, including the receptor model, the rate of Smad phosphorylation and h_0, h_1 and h_2, the receptor height parameters in the impulse model are highly correlated and are not identifiable individually. We assumed the rate of Smad phosphorylation was equal to unity and the parameter h_1 indicates both maximum receptor activity and rate of Smad phosphorylation. Smad2/3 phosphatase(s) are reported to be enriched in the nucleus and as in previous models (Schmierer, Tournier et al. 2008) the concentration of the Smad2/3 phosphatases can be set arbitrarily and for simplicity was set to unity. For Smad2/3 and pSmad2/3, the same import rate, k_{in} was considered (Schmierer, Tournier et al. 2008) but it was assumed that the complex of pSmad2/3-Smad4 has a different import rate, $k_{in\text{-}Complex}$. As our immunofluoresence results show (Figure 1) and as reported by (Schmierer, Tournier et al. 2008), the same import rate, k_{in} was considered for Smad2/3 and Smad4. In the absence of TGFβ, the only reactions taking place are constitutive nucleocytoplasmic shuttling of Smad2/3, Smad4 and Taz/Yap, which are all at steady state. The cytoplasmic/nuclear distributions of these proteins at steady state are defined by the ratio of export over import rates. As EpH4 cells express endogenous TGFβ, to establish steady state ratios in the absence of Smad phosphorylation, the ratio of import to export rates of Smads in cells treated with the TGFβ receptor inhibitor, SB-431542 were considered. Smad complex association and dissociation are assumed to take place in both the nucleus and cytoplasm and are reversible. The association/dissociation rates of pSmad2/3 and Smad4 are assumed to be equal in both the nucleus and cytoplasm (Schmierer, Tournier et al. 2008). However, these rates for the complex pSmad2/3-Smad4-Taz/Yap are different in the nucleus and cytoplasm. The nuclear import rate was fixed as k_{in} =9.36 h^{-1}, the rate measured by

(Schmierer, Tournier et al. 2008), though even if incorrect, the value scales all parameters by the same factor which is acceptable since we are comparing parameters at two conditions. We did not have absolute values of the protein masses, rather we used their relative values as percentages (see below), which is also appropriate as we will compare parameters in EpH4 cells transfected with siCTL versus siTaz/Yap. All experiments for the two conditions were carried out on the same plate and unknown model parameters at two conditions were estimated simultaneously. Since we used normalized mass values, the masses were unit-less and the units of the other parameters were changed accordingly. In the model for phosphorylation and dephosphorylation reactions, there was no obvious difference using either mass action law or Michaelis Menten kinetics, thus to reduce computational burden, we used the mass action law for all of the model reactions. During the 3 h modeling time period, there was no detectable protein turnover (Figure 2), hence, we assumed constant levels for Smad2/3, Smad4, Taz/Yap and receptors. Finally, we assumed that Smad3 undergoes identical reactions to Smad2 and there was no distinction between Smad2 and Smad3 in the process. A full description of the model parameters is given in Table S5.

Determination of Smad and Taz/Yap nuclear to cytoplasmic masses.

Automated immunofluorescence (IF) imaging was used to estimate the nuclear to cytoplasmic ratios of Smads and Taz/Yap since using ratios reduces intra assay variations and enables normalization of intensities in each individual IF plate. However, fluorescence data are proportional to concentrations, whereas immunoblot data are proportional to total particle numbers (Schmierer, Tournier et al. 2008). Thus, to determine protein masses, as required in the model, the estimated ratio was corrected for the ratio of nuclear to cytoplasmic volumes. Volume is base area times height, so as a rough approximation, the ratio of the volumes is the same as the ratio of the areas. To measure the areas, the number of pixels, each being 0.325 micrometers, covered by

nucleus, cytoplasm, and entire cell was determined. This revealed a ratio of cytoplasmic to nuclear volumes of 2.52 ± 0.023 for cells transfected with either siCTL or siT/Y, which is consistent with the previously reported value (Schmierer, Tournier et al. 2008). However, in the context of increasing cell density, cells are compressed and the nucleus, cytoplasmic and entire cell areas decrease yielding a decrease in the ratio at the highest cell density ($100x10^3$ cells/cm^2) to 1.25 ± 0.13. To estimate normalized cytoplasmic and nuclear masses as needed in the modeling process, the ratio, $R = \frac{C_{Nuc}}{C_{Cyt}} = \frac{M_{Nuc}/V_{Nuc}}{M_{Cyt}/V_{Cyt}}$, where C_{Nuc}, M_{Nuc}, V_{Nuc}, C_{Cyt}, M_{Cyt} and V_{Cyt} are nuclear and cytoplasmic concentrations, masses of the protein and volumes, respectively, was used. The ratio R and the ratio of nuclear to cytoplasmic volumes were measured by IF experiments and accordingly the ratio $R_m = \frac{M_{Nuc}}{M_{Cyt}}$ was calculated. Then, $1 + R_m = 1 + \frac{M_{Nuc}}{M_{Cyt}} = \frac{M_{Nuc}+M_{Cyt}}{M_{Cyt}}$. Since during signaling time period, it is assumed that there is no degradation of the proteins, by assuming $M_{Nuc} + M_{Cyt} = 100$, normalized cytoplasmic and nuclear masses of the proteins can be calculated as: $M_{Cyt} = \frac{100}{1+R_m}$ and $M_{Nuc} = \frac{100R_m}{1+R_m}$, respectively. The normalized masses of Smads in the nucleus and cytoplasm for cells transfected with siRNAs are shown in Figure S4. The masses of Taz/Yap in the cytoplasm and nucleus were similarly estimated. At low cell density, Taz/Yap mass was determined to be equally distributed whereas at high cell density it is 60 and 40 percent in the cytoplasm versus nucleus, respectively.

Parameter estimation, identifiability, residual analysis and model selection.

To estimate the unknown model parameters in the different scenarios, the $DREAM_{(ZS)}$ algorithm was used (Vrugt, Ter Braak et al. 2008a, Vrugt, Ter Braak et al. 2009, Vrugta 2016) with five Markov chains and uniform prior distributions for the unknown parameters, and dependent on the model complexity, on average 500000-1000000 samples. The log-likelihood function was a

Gaussian likelihood in which the measurement errors were considered explicitly. Convergence of Markov chains in each case was confirmed as the $\hat{R}$-statistic for all parameters dropping below 1.2. The $\hat{R}$-statistic of Gelman et al. (Gelman and Rubin 1992) was employed, which calculates the ratio of between-chain variance to within chain variance to assure the convergence of the algorithm. The threshold of $\hat{R}$=1.2 was applied for convergence diagnosis of the DREAM$_{(ZS)}$ algorithm. After convergence, the last 25% of the samples in each chain were utilized to summarize the posterior distribution accounting for the burn-in period. To analyze identifiability of parameters of the model, we estimated profile likelihoods of the model parameters using DREAM$_{(ZS)}$ with 5 Markov chains. Residual analysis was determined using MATLAB software. Residuals are differences between the model output and the measured output. Thus, residuals represent the portion of the validation data not explained by the model. A good model has the residual autocorrelation function inside the confidence interval of the corresponding estimates, indicating that the residuals are uncorrelated. To check, the residual autocorrelation function was plotted for each model fitting. On the other hand, the residuals are assumed to be random variables and normally distributed. To check this, error residuals were plotted over the model predicted outputs to confirm they show no fitted pattern. The normal quantile-quantile plots of the residuals were plotted to investigate if they follow approximately a straight line, to confirm that the residuals are normally distributed. Finally, to find the best model among those proposed the Bayesian model averaging (BMA) (Vrugt, Diks et al. 2008b) was used.

Determination of Initial Conditions.

To find the initial concentrations of phosphorylated Smads and receptors, which are at non-zero in the basal state, their steady state levels in the absence of TGFβ, where the derivatives of concentrations of different proteins were equal to zero was calculated (Strasen, Sarma et al. 2018).

At each iteration of DREAM$_{(ZS)}$ algorithm, the unknown initial values were estimated alongside with other unknown parameters of the model. To do this, the derivatives of the state variables were equal to zero, the initial value of receptor was set as $(h_0 + \frac{(h_1-h_0)}{(1+\exp(\beta_1 t_1))})(h_2 + \frac{(h_1-h_2)}{(1+\exp(-\beta_2 t_2))})/h_1$ and totals of the different complexes of Smads were set to initial values measured by IF experiments. Using the simplex search method (Lagarias, Reeds et al. 1998), with the MATLAB fmincon command to solve a system of nonlinear equations for each set of parameters, the initial values of cytoplasmic and nuclear signals and the parameter h_0 were calculated.

The simplified model: statistical analysis and behavior of residuals.

For statistical analysis of the estimated parameters and initial values for the simplified model (Table S11 and S12) the Chi-Square goodness of fit test (McDonald 2009) was used to measure how well the data fit the predictions of the given model. The Chi squared statistic of the simplified model, $\chi^2 = 0.5609$ was less than the critical value of χ^2 with $\upsilon = 18$ degrees of freedom and $p = 0.01$, (CV= 7.01), indicating that the model fit the data appropriately. Next, the identified model was validated by checking the behaviour of the residuals. The residual autocorrelation function of the model was inside the confidence interval of the corresponding estimates, indicating that the residuals are uncorrelated and the whiteness test was fulfilled (Figure S5). Plotting of the model residuals over the model predicted outputs and the quantile-quantile plots confirmed that the model residuals are random variables, which approximately follow Gaussian distribution (Figure S5B). On the other hand, the parameter correlation matrix (Table S13) showed there was no strong correlation between the estimated parameters, which confirmed unique parameter estimation. The receptor activity for the best fitted parameter values revealed that the maximum activity occurred around 1.3 h and thereafter due to negative regulation, the receptor activity declined (Figure S5B).

In the identified model, the pSmad2/3-Smad4 complex had a lifetime of less than 1 min. The complex of pSmad2/3-Smad4 had higher affinity for Taz/Yap in the cytoplasm than in the nucleus. However, the interaction was more stable in the nucleus, presumably due to nuclear retention factors. The import rate of the complex pSmad2/3-Smad4 was on average 16 times larger than that of Smad2/3 or Smad4. The 95% uncertainty ranges for the model simulation data due to total and parameter uncertainties (Figure S5B), confirmed that the process dynamics are well captured by the model.

Receptor Activity Alteration (RAA) hypothesis: statistical analysis and behavior of residuals. For the Receptor Activity Alteration (RAA) model, except for the receptors, all other parameters were the same in the two conditions and were estimated using $\text{DREAM}_{(ZS)}$. The statistical analysis of the estimated parameters and initial values are given in Tables S14 and S15, (left three columns), respectively. The Chi squared statistic of the model, $\chi^2 = 2.5363$ is less than the critical value of χ^2 with $\upsilon = 48$ degrees of freedom and $p = 0.01$, (CV= 28.177), indicating that the model fits the data appropriately. The autocorrelation of residuals shows that the residuals are all within the confidence interval, uncorrelated and random variables with approximately normal distribution (Figure S6). The correlation matrix of the estimated parameters (Table S16) confirms there are no strong correlations between parameters. The estimated parameter values show that the parameters h_0, h_1, h_2, t_1, β_1 and β_2 of the receptors at two conditions have the same probability distribution and only the parameter t_2 differs at two conditions. To test whether a restricted model with all parameters the same, except the parameter t_2 at two conditions, explain the data, model parameters were estimated assuming that the 6 aforementioned parameters in the receptor models are the same. The model fitted the data very well based on the goodness of fit test, as $\chi^2 = 2.496$ is less than the critical value of χ^2 with $\upsilon = 53$ degrees of freedom and $p = 0.01$, (CV= 32.0185). The residual

analysis of the restricted model also validates the model (Figure S6). The correlation matrix of the estimated parameters (Table S17) confirms there is no strong correlation between parameters. The restricted model differs from the full model by the removal of six additional receptor parameters.

Using the Bayesian Model Averaging (BMA) strategy (Vrugt, Diks et al. 2008b) the estimated weights for the restricted and full modes are 0.757±0.223 and 0.242±0.223, respectively, which strongly rejects the full model in favour of the restricted model. In this case the full model does not fit the data significantly better than the restricted model, and we infer that the six additional receptor parameters are not biologically meaningful. The maximum a posteriori (MAP) values (Figure S6) indicate that for both conditions the receptors have the same activity, however near the peak, receptor activity in siTaz/Yap declines faster (Figures 1 and 3). The proposed hypothesis suggests that the same negative regulation exists in both control and cells lacking Taz/Yap. However, in siTaz/Yap transfected cells, the mechanism triggers 1.2435±0.1391 h sooner. To quantify receptor activity at each condition, the integral of time course curve was calculated via the trapezoidal method provided in MATLAB. On average, in the restricted model, the receptors in control cells are 1.4759±0.0673 times more active compared to siTaz/Yap transfected cells. The 95% uncertainty ranges for the simulation data for the full and restricted RAA models is shown in (Figure S6). In the selected model, the dissociation rate of the complex of pSmad2/3-Smad4 is around 68.7875 h^{-1} corresponding to a mean complex lifetime of around one minute and the import rate of the complex pSmad2/3-Smad4 is roughly 5 times larger than that of Smad2/3, Smad4 or pSmad2/3. These results are in agreement with a previous report (Schmierer, Tournier et al. 2008).

Nuclear Retention Factor hypotheses (CRF and DRF): statistical analysis and behavior of residuals.

For the Nuclear Retention Factor hypotheses, the receptor activity parameters do not change but there is an unknown factor (X) in the nucleus, which we assumed for simplicity, had a constant concentration (Figure 5C). Two scenarios were considered, first, Factor X is constant regardless of siRNA transfection, the Constant Retention Factor (CRF) model and second where the expression level of X is downregulated by a factor α, in the range [0 1] in siTaz/Yap transfected cells, the Down Regulated Retention Factor (DRF) model. Statistical analysis of the estimated process parameters and initial values for the two proposed models are provided in Tables S18 and S19. The χ^2 statistic of the CRF and DRF models are 2.8291 and 2.66, respectively and are less than the critical values of χ^2 with 48 and 47 degrees of freedom and p = 0.01 (28.18 and 27.41) which confirms that the data fit the models well. The residuals analyses for both models are uncorrelated random variables with approximately normal distribution, validating the models (Figure S7). The correlation matrices of the estimated parameters for the two models are summarized in Tables S20 and S21. The temporal receptor patterns show that in both models the receptors have the same activity at two conditions (Figure S7). The 95% uncertainty ranges for the simulation data for the CRF and DRF models confirm that the process dynamics are captured by the models (Figure S7). In the DRF model, Factor X is reduced by more than 60%. In both models, the mean complex lifetimes of the complex pSmad2/3-Smad4 is less than 1 min and the import rate of the complex pSmad2/3-Smad4 is roughly 15 and 12 times larger than that of Smad2/3, Smad4 or pSmad2/3 in the CRF and DRF models, respectively. The estimated weights for the CRF and DRF using the BMA strategy are 0.725±0.165 and 0.274 ± 0.165, respectively, which rejects the DRF in favor of CRF.

Receptor Activity Alteration-Constant Retention Factor (RAACRF) and Receptor Activity Alteration-Downregulated Retention Factor (RAADRF): statistical analysis and behavior of residuals.

To determine whether both receptor activity alterations as well as the presence of a nuclear retention factor are valid, we investigated models in which both receptor parameters change and a nuclear retention factor changes with either constant levels (RAACRF) or with levels downregulated in siTaz/Yap transfected cells (RAADRF) (Figure 5C). Statistical analysis of the estimated parameters and the initial values for different signals in the models are given in Tables S22 and S23, respectively. The χ^2 statistic of the RAACRF and RAADRF models are 2.4605 and 2.469, respectively and are less than the critical values of χ^2 with 46 and 45 degrees of freedom and p = 0.01 (26.66 and 25.9) which confirms that the data fits the models well. The residual analysis validates both models (Figure S8). The receptor activity declines by the same slope in cells transfected with siCTL or siTaz/Yap. However, in cells transfected with siTaz/Yap, receptor activity declines on average 1 h sooner (1.045± 0.3447 h in RAACRF and 0.9302± 0.2206 h in RAADRF) (Figure S8). In both models, the retention factor X stabilizes the complex pSmad2/3-Smad4-Taz/Yap. However in the RAADRF model, Factor X is reduced by 24.3647± 6.4869%. The 95% uncertainty ranges for the simulation data for the RAACRF and RAADRF models are shown in Figure S8. The matrix of parameter correlation for both models confirms that there is no strong correlation between parameters guaranteeing unique parameter identification (Tables S24 and S25).

Code availability. The $\text{DREAM}_{(ZS)}$ package is available for download (https://www.pc-progress.com/en/Default.aspx?jasper-vrugt) and Matlab codes used in this study will be provided upon request.

REFERENCES

Chechik, G. and D. Koller (2009). "Timing of gene expression responses to environmental changes." *J Comput Biol* **16**(2): 279-290.

Edelstein-Keshet, L. (2005). *Mathematical models in biology*, SIAM, doi.org/10.1137/1.9780898719147.

Gelman, A. and J. Hill (2006). Data analysis using regression and multilevel/hierarchical models, Cambridge University Press.

Gelman, A. and D. B. Rubin (1992). "Inference from iterative simulation using multiple sequences." *Statistical science* **7**(4): 457-472.

Hox, J. J., M. Moerbeek and R. Van de Schoot (2017). Multilevel analysis: Techniques and applications, Routledge.

Labbe, E., A. Letamendia and L. Attisano (2000). "Association of Smads with lymphoid enhancer binding factor 1/T cell-specific factor mediates cooperative signaling by the transforming growth factor-beta and wnt pathways." *Proc Natl Acad Sci U S A* **97**(15): 8358-8363.

Lagarias, J. C., J. A. Reeds, M. H. Wright and P. E. Wright (1998). "Convergence properties of the Nelder--Mead simplex method in low dimensions." *SIAM Journal on Optimization* **9**(1): 112-147.

McDonald, J. H. (2009). Handbook of biological statistics, Sparky House Publishing Baltimore.

Moustakas, A. and C. H. Heldin (2009). "The regulation of TGFbeta signal transduction." *Development* **136**(22): 3699-3714.

Oida, T. and H. L. Weiner (2010). "TGF-beta induces surface LAP expression on murine CD4 T cells independent of Foxp3 induction." *PLoS One* **5**(11): e15523.

Pinero, J. and D. Bates (2000). Mixed-effects models in S and S-PLUS (Statistics and Computing), Springer, New York.

Schmierer, B., A. L. Tournier, P. A. Bates and C. S. Hill (2008). "Mathematical modeling identifies Smad nucleocytoplasmic shuttling as a dynamic signal-interpreting system." *Proc Natl Acad Sci U S A* **105**(18): 6608-6613.

Strasen, J., U. Sarma, M. Jentsch, S. Bohn, C. Sheng, D. Horbelt, P. Knaus, S. Legewie and A. Loewer (2018). "Cell-specific responses to the cytokine TGFbeta are determined by variability in protein levels." *Mol Syst Biol* **14**(1): e7733.

Vrugt, J. A., C. J. Ter Braak, M. P. Clark, J. M. Hyman and B. A. Robinson (2008a). "Treatment of input uncertainty in hydrologic modeling: Doing hydrology backward with Markov chain Monte Carlo simulation." *Water Resources Research* **44**(12). doi.org/10.1029/2007WR006720

Vrugt, J. A., C. G. Diks and M. P. Clark (2008b). "Ensemble Bayesian model averaging using Markov chain Monte Carlo sampling." *Environmental Fluid Mechanics* **8**(5-6): 579-595.

Vrugt, J. A., C. Ter Braak, C. Diks, B. A. Robinson, J. M. Hyman and D. Higdon (2009). "Accelerating Markov chain Monte Carlo simulation by differential evolution with self-adaptive randomized subspace sampling." *International Journal of Nonlinear Sciences and Numerical Simulation* **10**(3): 273-290.

Vrugt, J. A. (2016). "Markov chain Monte Carlo simulation using the DREAM software package: Theory, concepts, and MATLAB implementation." *Environmental Modelling & Software* **75**: 273-316.